JOURNAL OF COMPUTATIONAL PHYSICS 89, 125–160 (1990)

An Artificial Compression Method for ENO Schemes: The Slope Modification Method

HUANAN YANG*

Department of Mathematics, UCLA, Los Angeles, California 90024

Received September 26, 1988; revised February 13, 1989

A simple and efficient method of artificial compression is introduced. This method is based on a modification of the slopes of the ENO reconstruction and, with the help of suitably chosen parameters, greatly improves the resolution of the contact discontinuities. Numerical examples are provided to test the performance of the method and to give some suggestions as to the choice of the parameters. © 1990 Academic Press, Inc.

1. INTRODUCTION

In this paper, we introduce a simple yet effective method to improve the performance of the ENO schemes for hyperbolic conservation laws.

Consider the following initial value problem:

$$\begin{aligned} &u_t + f(u)_x = 0 \\ &u(x, 0) = u_0(x), \end{aligned} \tag{1.1}$$

where u is a vector function of one space dimension and time, and f is a vector function of u.

Assume that the system (1.1) is strictly hyperbolic in the sense that the Jacobian

$$A = \frac{\partial f}{\partial u} \tag{1.2}$$

has only real eigenvalues with a complete set of eigenvectors.

It is well known that the solution of (1.1) may develop discontinuities in finite time even though the initial value $u_0(x)$ is very smooth, say, a C^∞ function. These discontinuities include shocks, contact discontinuities, and the wave fronts of rarefaction waves.

It is natural that efforts in numerically simulating the solution of (1.1) with these

* Research partially supported by ONR Grant N0014-86-K-0691, NSF Grant DMS 85-03294, NASA Langley Grant NAG1-270, and AFOSR Grant F49620-86-C-0115.

0021-9991/90 $3.00

structures mainly focus on designing numerical schemes with the following properties:

(i) achieving high accuracy in smooth regions of the solutions,

(ii) producing sharp profiles for the shocks and the contact discontinuities,

(iii) avoiding superfluous oscillations in front of or behind the shocks and the contact discontinuities,

(iv) getting correct positions and speed of the discontinuities, and

(v) avoiding non-physical discontinuities (e.g., expansion shocks).

The Lax–Wendroff theorem (see [13]) says that, for a convergent conservative scheme consistent with (1.1), the limit function of the numerical solution as the mesh size tends to zero is a weak solution of (1.1). Thus, conservative schemes automatically guarantees (iv). Throughout this paper, we shall only consider schemes in conservation form.

To enforce (v), one has to consider the so called entropy conditions which distinguish the physical solution from others. However, we are not going to discuss this problem here.

Recently, Harten, Osher, Engquist, and Chakravarthy (see [2–4]) introduced a class of essentially non-oscillatory (ENO) schemes which are of globally high order of accuracy where the solution is smooth. Although a complete theoretical analysis of these schemes has not been done, extensive numerical examples show that these schemes are nonlinearly stable. Hence, these schemes excellently meet the requirements (i) and (iii). For (ii), the ENO schemes produce extremely sharp shock profiles. However, they smear the contact discontinuities at a rate which appears to be of order $O(n^{1/(r+1)})$, where r is the order of accuracy, and n is the number of the time steps. In order to overcome this difficulty, Harten introduced the concept of subcell resolution. This led to excellent results in 1d computation. He is currently considering 2d extensions. Another method which can be used to sharpen the contact discontinuity is Mao's method introduced in [11]. Merging his ideas with subcell resolution, Mao's method, hopefully, could be used with any known scheme. Some remarkable results have been obtained. However, much work needs to be done in order to make it practical in the cases of systems and of multidimensions.

In this paper we will introduce a procedure which is different from Harten's and Mao's and which greatly improves the performance of the ENO schemes at the contact discontinuities. This is going to be achieved by combining the ENO schemes with an ACM (artificial compression method, see Harten's pioneering work [1]) type technique. In this way, we can effectively prevent the contact discontinuities from being smeared and, in most cases, limit the transition of a numerically computed contact discontinuity to about two cells while essentially keeping the order of accuracy in the smooth regions of the solutions.

This procedure was originally invented for the cell average framework of the ENO schemes. Since then, Shu and Osher have transformed it to their pointwise

ENO schemes. They have obtained surprisingly good results in 2d computations. See [7] for the details.

In the next section, we will give a brief review of the ENO schemes. Section 3 describes in detail our ACM type technique—the slope modification method and proves some of its properties. Section 4 applies the method to the system of Euler equations for gas dynamics. In Section 5, we will present some numerical results showing the performance of our method as well as giving some suggestions as to the choice of the parameters concerned.

2. Review of the ENO Schemes

We refer to [2–8] for details of the cell average ENO schemes and their pointwise versions. Here we only give a very brief review of the schemes. This is necessary for us to describe our slope modification method.

Originally, the ENO schemes were introduced for cell average values of the solutions as high order extensions of the Godunov scheme at the MUSCL scheme. Denote by v the numerical solution approximating the sliding average $\bar{u}$ of the exact solution u of (1.1), i.e.,

$$v(x, t) \doteq \bar{u}(x, t) = \frac{1}{h}\int_{x-h/2}^{x+h/2} u(y, t)\, dy.$$

Let $\{[x_{j-1/2}, x_{j+1/2}] \times [t_n, t_{n+1}]\}$, where $x_\alpha = \alpha h$, $t_n = n\tau$, $j = 0, \pm 1, \pm 2, \ldots$, $n = 0, 1, 2, \ldots$, be a partition of $\mathbf{R} \times \mathbf{R}^+$. Denote $u(x_j, t_n)$ by u_j^n and $v(x_j, t_n)$ by v_j^n. Assume that $E(t)$ is the exact solution operator of (1.1). I.e., if $u(x, t)$ is the solution of (1.1), then

$$u(x, t) = E(t)\, u(x, 0).$$

The theoretical ENO scheme can be written as

$$v_j^{n+1} = \frac{1}{h}\int_{x_{j-1/2}}^{x_{j+1/2}} E(\tau)\, R(x, v^n)\, dx \tag{2.1}$$

which is said to be "theoretical," since $E(t)$ is exact. In (2.1), $R(x, v^n)$ is a pointwise approximation of the solution u at time t^n derived from the cell average approximate solution v^n. It is a piecewise polynomial. In fact, it is a polynomial in each cell $(x_{j-1/2}, x_{j+1/2})$. The procedure of computing $R(x, v^n)$ from v^n is called reconstruction.

Given the cell averages $\{v_j\}_{j=-\infty}^{\infty}$ of a function $u(x)$, in [3] two ways to compute $R(x, v^n)$, reconstruction via primitive function (RP) and reconstruction via decon-

volution (RD) were described. We only review RP here since a knowledge of it is enough for us to introduce our slope modification method.

Notice that, for any fixed integer i_0, $\{p_i\}_{i=i_0}^{\infty} = \{\sum_{j=i_0}^{i} v_j h\}_{i=i_0}^{\infty}$ is a sequence of pointwise values of the primitive function $p(x) = \int_{x_{i_0-1/2}}^{x} u(x)\,dx$ of $u(x)$ at $x_{i_0-1/2}$, $x_{i_0+1/2}$, $x_{i_0+3/2}$, ... A natural way of getting a polynomial which approximates u in the cell $(x_{j-1/2}, x_{j+1/2})$ is, therefore, to interpolate $p(x)$ at $r+1$ consecutive points $x_{i(j)-1/2}$, $x_{i(j)+1/2}$, ..., $x_{i(j)+r+1/2}$, including $x_{j-1/2}$ and $x_{j+1/2}$. The derivatives of the interpolating polynomial then give the reconstruction and its derivatives. One has r degrees of freedom of choosing $i(j)$, i.e., the stencil. It is the way of choosing the stencil that distinguishes the ENO schemes from others.

For simplicity, we only give the hierarchical algorithm for evaluating $i(j)$. The goal is to find the "smoothest" stencil which includes $x_{j-1/2}$ and $x_{j+1/2}$. The smoothness of the stencil is somehow measured by the absolute value of the divided differences $p[x_j, x_{j+1}, ..., x_{j+k}]$ which are defined inductively by

$$p[x_j] = p(x_j), \qquad j = -\infty, ..., +\infty, \tag{2.2}$$

and

$$p[x_j, x_{j+1}, ..., x_{j+k}] = (p[x_{j+1}, ..., x_{j+k}] - p[x_j, ..., x_{j+k-1}])/(x_{j+k} - x_j),$$
$$k = 1, 2, ..., r \tag{2.3}$$
$$i = -\infty, ..., \infty.$$

We describe the algorithm evaluating $i(j)$ in the flavor of Fortran language as follows:

(1) $i(j) = j$.

(2) For $k = 1, 2, ..., r$, if

$$|p[x_{i(j)-1-1/2}, ..., x_{i(j)-1-1/2+k}]| \leqslant |p[x_{i(j)-1/2}, ..., x_{i(j)-1/2+k}]|,$$

then

$$i(j) = i(j) - 1.$$

Having computed $i(j)$, one then gets a polynomial $p_j(x, v)$ by Newton's form of interpolation. From this the reconstruction $R(x, v)$ and its derivatives at $x = x_j$ are given by

$$\frac{d^l}{dx^l} R(x, v)|_{x=x_j} = \frac{d^{l+1}}{dx^{l+1}} p_j(x, v)|_{x=x_j}, \qquad l = 0, 1, ..., r-1.$$

3. The Slope Modification Method for Scalar Conservation Laws

Denote by $\delta_{j-1/2}$ the jump of $R(x, v)$ at the cell interface $x_{j-1/2}$, i.e.,

$$\delta_{j-1/2} = R(x_{j-1/2} + 0, v) - R(x_{j-1/2} - 0, v). \tag{3.1}$$

We introduce the following slope modification algorithm:

ALGORITHM 3.1. The modified reconstruction $\hat{R}(x, v)$ in $(x_{j-1/2}, x_{j+1/2})$ is a $(r-1)$th order polynomial which is defined by

$$\frac{d^l}{dx^l}\hat{R}(x, v)|_{x=x_j} = \frac{d^l}{dx^l}R(x, v)|_{x=x_j}, \qquad l \leqslant r-1, l \neq 1, \tag{3.2}$$

$$\frac{d}{dx}\hat{R}(x, v)|_{x=x_j} = \frac{d}{dx}R(x, v)|_{x=x_j} + \partial S_j/h, \tag{3.3}$$

where the slope modifier ∂S_j is given by

$$\partial S_j = 2\mathrm{m}(\alpha_j \mathrm{m}(\delta_{j-1/2}, \delta_{j+1/2}), \mathrm{m}(v_{j+1} - R^-_{j+1/2}, R^+_{j-1/2} - v_{j-1})); \tag{3.4}$$

here $\{\alpha_j\}$ is a sequence of positive numbers, the function $\mathrm{m}(x, y)$ is defined by

$$\mathrm{m}(x, y) = \begin{cases} 0, & xy \leqslant 0, \\ \min(|x|, |y|)\,\mathrm{sgn}(x), & \text{otherwise}, \end{cases} \tag{3.5}$$

and $R^{\pm}_{j+1/2}$ denotes $R(x_{j+1/2} \pm 0, v)$.

To see the effect of the algorithm, let us apply it to the UNO scheme introduced in [1]. The UNO scheme is based on a non-oscillatory piecewise linear reconstruction. More precisely, if $v = \{v_j\}_{j=-\infty}^{\infty}$ are the cell averages of a function u, the UNO reconstruction $R(x, v)$ can be written as

$$R(x, v) = v_j + S_j \frac{x - x_j}{h}, \qquad x_{j-1/2} < x < x_{j+1/2}. \tag{3.6}$$

The reconstruction is non-oscillatory in the sense that the number of the extrema of $R(\cdot, v)$ is no more than that of v. We recall that $R(\cdot, v)$ satisfies (see [2])

$$\delta_{j-1/2}(v_j - v_{j-1}) \geqslant 0, \tag{3.7}$$

$$\delta_{j-1/2} = 0, \qquad \text{if} \quad v_j - v_{j-1} = 0, \tag{3.8}$$

$$S_j \mathrm{m}(v_{j+1} - v_j, v_j - v_{j-1}) \geqslant 0. \tag{3.9}$$

Recall also that (see [1]), if the numerical scheme for scalar conservation law (1.1) is

$$v_j^{n+1} = v_j^n - \lambda(\hat{f}_{j+1/2} - \hat{f}_{j-1/2}), \tag{3.10}$$

a modified scheme adding artificial compression to (3.10) would be

$$v_j^{n+1} = v_j^n - \lambda(\bar{f}_{j+1/2} - \bar{f}_{j-1/2}), \tag{3.11}$$

where the flux modifier

$$g_{j+1/2} = \bar{f}_{j+1/2} - \hat{f}_{j+1/2} \tag{3.12}$$

obeys

$$g_{j+1/2}\,\Delta v_j^n \geqslant 0. \tag{3.13}$$

Consider the UNO scheme with numerical flux (see [2])

$$\hat{f}_{j+1/2} = \begin{cases} f(v_j^n) + 0.5\bar{a}_{j+1/2}(1-\lambda\bar{a}_{j-1/2})S_j^n/[1+\lambda(\bar{a}_{j+1/2}-\bar{a}_{j-1/2})] \\ \qquad \text{if} \quad \bar{a}_{j+1/2} \geqslant 0, \\ f(v_{j+1}^n) - 0.5\bar{a}_{j+1/2}(1+\lambda\bar{a}_{j+3/2})S_{j+1}^n/[1+\lambda(\bar{a}_{j+3/2}-\bar{a}_{j+1/2})] \\ \qquad \text{if} \quad \bar{a}_{j+1/2} < 0, \end{cases} \tag{3.14}$$

where

$$\bar{a}_{j+1/2} = (f(v_{j+1}^n) - f(v_j^n))/(v_{j+1}^n - v_j^n). \tag{3.15}$$

In the remaining part of this section, by "the UNO scheme," we always mean the scheme with this flux.

Applying the slope modification method to the UNO scheme, one gets a scheme whose numerical flux has the same expression as (3.14) except that S_j is replaced by $\hat{S}_j$ for all j.

From (3.4), (3.7), (3.8), and (3.13) one can see that under the CFL type conditions

$$|\lambda\bar{a}_{j+1/2}| < 1 \tag{3.16}$$

and

$$\lambda(\bar{a}_{j+1/2} - \bar{a}_{j-1/2}) > -1, \tag{3.17}$$

Algorithm 3.1 applied to the UNO scheme has the effect of adding artificial compression to the UNO scheme.

Remark 3.2. For general high order ENO schemes, (3.7)–(3.9) are not necessarily true. Nevertheless, the numerical experiments in [4] (see the figures of the reconstructions at the end of [4]) show that they are essentially true. Furthermore, the numerical results we are going to report in Section 5, show that the slope modifier with suitably chosen α_j works well for all the cases that we have tested, although a rigorous analysis is not available now.

Next, we discuss the stability of our method. Since the modified reconstruction no longer obeys (3.7)–(3.9), the algorithm does introduce oscillations to the reconstruction. However, due to the cell average process, it seldom introduces oscillations to the solution at the next time level. In fact, we have

THEOREM 3.3. *If* $\lambda\,|\bar{a}_{j+1/2} - \bar{a}_{j-1/2}| < 1$ *and* $\lambda\,|\bar{a}_{j+1/2}| < 1$ *hold for all* j, *then the modified scheme obtained by applying Algorithm* 3.1 *to the UNO scheme is non-oscillatory.*

For a proof of the theorem, we refer the interested readers to the author's thesis [16].

Remark 3.4. For general ENO schemes, of course, the conclusion of Theorem 3.3 no longer holds. However, according to our numerical experiments, we believe that the modified ENO schemes obtained by applying Algorithm 3.1 is still essentially non-oscillatory.

Now, we consider the order of accuracy of our method. For linear equation

$$u_t + u_x = 0,$$

we have

THEOREM 3.5. *Suppose the α_j's in Algorithm* 3.1 *are uniformly bounded, then at the worst, this method lowers the accuracy of the original scheme by one order. If, in addition,*

$$\alpha_{j+1} - \alpha_j = O(h),$$

then the method applied to the ENO schemes keeps the order of the accuracy. For the choices of the parameters we are going to suggest, this last condition is valid if there are no zeros of the first $r-1$ derivatives of the true solution u near x_j.

Proof. It suffices to recall that, at the cell interface $x_{j+1/2}$, the jump $\delta_{j+1/2}$ of the reconstruction satisfies

$$\delta_{j+1/2} = c_{j+1/2} h^r + O(h^{r+1}) \tag{3.18}$$

and

$$\Delta c_{j+1/2} = O(h) \tag{3.19}$$

if

$$\left(\frac{d}{dx}\right)^l u(x) \neq 0, \qquad l = 1, 2, \ldots, r-1.$$

We believe that the conclusion of the above theorem is also true for the fully non-linear problems, but do not have a proof yet.

Next, we discuss the choice of the α_j's. Hereafter we shall call them the SM (slope modification) coefficients. Unfortunately, we have not been above to give a universal method for determining the α_j's. The recommendations we are going to give come from our numerical experiments. We found that, for linear problems, the smearing effect is essentially eliminated when the α_j's are greater than or equal to 1.9–2.3. One usually gets satisfactory results by letting α_j be equal to or slightly larger than the smallest number capable of eliminating the smearing effect.

For the problems with rich smooth structures, the uniform choice of α_j as suggested above could run into trouble. Although the essentially non-oscillatory

property is generally kept, some artificial contact discontinuities may damage the smooth structure.

One way of avoiding this is to use a discontinuity detector. A well known one is

$$\mu_j = \left(\frac{\Delta^2 u_{j-1}}{|\Delta u_{j-1}| + |\Delta u_j|} \right)^2. \tag{3.20}$$

Then α_j can be written as

$$\alpha_j = c\mu_j \tag{3.21}$$

In most computations we have performed, $c = 33$.

Remark 3.6. Usually, (3.20) and (3.21) give satisfactory results. However, for the local CFL number far away from ± 0.5, the compression effect is not balanced between the head and the tail of a discontinuity. Further improvement can be made by multiplying the coefficients (3.21) with a balance factor. For details of the balance factor, see Section 5.

4. Application to the ENO Schemes for the Euler Equations of Gas Dynamics

In this section, we apply the slope modification method to the ENO schemes for the Euler equations of gas dynamics for a polytropic gas. The application to the general systems of hyperbolic conservation laws follows immediately.

For a polytropic gas, the governing equations are, as in [4],

$$u_t + f(u)_x = 0 \tag{4.1}$$

$$u = (\rho, m, E)^T \tag{4.2}$$

$$f(u) = qu + (0, P, qP)^T \tag{4.3}$$

$$P = (\gamma - 1)(E - \tfrac{1}{2}\rho q^2). \tag{4.4}$$

Here ρ, q, P, and E are the density, velocity, pressure, and total energy, respectively; $m = \rho q$ is the momentum and γ is the ratio of specific heats.

The eigenvalues of the Jacobian matrix $\partial f/\partial u$ are

$$a_1(u) = q - c, \qquad a_2(u) = q, \qquad a_3(u) = q + c, \tag{4.5}$$

where $c = (\gamma P/\rho)^{1/2}$ is the sound speed.

The corresponding right-eigenvectors are

$$r_1(u) = \begin{pmatrix} 1 \\ q - c \\ H - qc \end{pmatrix}, \qquad r_2(u) = \begin{pmatrix} 1 \\ q \\ \frac{1}{2}q^2 \end{pmatrix}, \qquad r_3(u) = \begin{pmatrix} 1 \\ q + c \\ H + qc \end{pmatrix}; \tag{4.6}$$

here

$$H = (E+P)/\rho = c^2/(\gamma-1) + \tfrac{1}{2}q^2 \tag{4.7}$$

is the enthalpy.

The corresponding left-eigenvectors bi-orthonormal to (2.53) are

$$\begin{aligned} l_1(u) &= \tfrac{1}{2}(b_2 + q/c,\ -b_1 q - 1/c,\ b_1) \\ l_2(u) &= (1-b_2,\ b_1 q,\ -b_1) \\ l_3(u) &= \tfrac{1}{2}(b_2 - q/c,\ -b_1 q + 1/c,\ b_1), \end{aligned} \tag{4.8}$$

where

$$b_1 = (\gamma-1)/c^2 \tag{4.9}$$

$$b_2 = \tfrac{1}{2}q^2 b_1. \tag{4.10}$$

To avoid too many collisions of the discontinuities which damage the advantage of the ENO reconstructions, ENO uses the characteristic reconstruction. Numerical experiments demonstrate that our slope modifier should also be applied in characteristic variables to get rid of some, although minor, spurious oscillations. In addition, since our goal is to sharpen the contact discontinuities which are the 2-waves, we only have to use it in the second field. We now introduce two algorithms to modify the rth order characteristic reconstruction.

ALGORITHM 2.11. For each j,

(1) Compute the locally defined characteristic variables

$$\begin{aligned} \bar{w}_i^k(v_j^n) = l_k(v_j^n) v_i^n \qquad &\text{for} \quad i = j-r, \ldots, j+r \text{ if } k = 1, 3, \\ &\text{for} \quad i = j-r-1, \ldots, j+r+1 \text{ if } k = 2. \end{aligned} \tag{4.11}$$

(2) Apply the scalar reconstruction algorithm to each of the locally defined characteristic variables in (4.11). The result is

$$b_{j,l}^k = \frac{\partial^l}{\partial x^l} R(x; \bar{w}^k(v_j^n))|_{x=x_j}, \qquad l = 0, 1, \ldots, r-1;\ k = 1, 3, \tag{4.12}$$

and

$$\frac{\partial^l}{\partial x^l} R(x; \bar{w}^2(v_j^n))|_{x=x_{j+m}}, \qquad l = 0, 1, \ldots, r-1;\ m = -1, 0, 1. \tag{4.13}$$

When $m = 0$, $l \neq 1$, we denote (4.13) by $b_{j,l}^2$.

(3) Apply our method, i.e., add the slope modifier to (4.13) to get $b_{j,1}^2$.

(4) Transform back to physical variables:

$$R(x; v^n) = \sum_{l=0}^{r-1} \mathbf{b}_{j,l}(x - x_j)^l / l!, \qquad x_{j-1/2} < x < x_{j+1/2}, \tag{4.14}$$

where

$$\mathbf{b}_{j,l} = \sum_{k=1}^{3} b_{j,l}^k r_k. \tag{4.15}$$

ALGORITHM 2.12. (1) For each j, do the ENO characteristic reconstruction as usual to get $R(x, v^n)$ for $x_{j-1/2} < x < x_{j+1/2}$. Store $l_2(v_j^n)$, $r_2(v_j^n)$, $\bar{w}_{j-1}^2(v_j^n)$, $\bar{w}_j^2(v_j^n)$, $\bar{w}_{j+1}^2(v_j^n)$, and $b_{j,l}^2$.

(2) For each j, compute $R_{j+1/2}^{\pm} = R(x_{j+1/2} \pm 0, v^n)$, $\delta_{j+1/2} = R_{j+1/2}^{+} - R_{j+1/2}^{-}$.

(3) For each j,

(i) compute

$$R^+(w) = l_2(v_j) R_{j+1/2}^-,$$
$$R^-(w) = l_2(v_j) R_{j-1/2}^+,$$
$$\delta^+(w) = l_2(v_j)\, \delta_{j+1/2},$$

and

$$\delta^-(w) = l_2(v_j)\, \delta_{j-1/2};$$

(ii) using $\bar{w}_{j-1}^2(v_j^n)$, $\bar{w}_j^2(v_j^n)$, $\bar{w}_{j+1}^2(v_j^n)$, $R^+(w)$, $R^-(w)$, $\delta^+(w)$, and $\delta^-(w)$ to get the slope modifier $\partial b_{j,1}^2$,

(iii) compute $\mathbf{b}_{j,1} = \mathbf{b}_{j,1} + \partial b_{j,1}^2 r_2(v_j^n)$.

5. NUMERICAL RESULTS

Since our purpose in designing the slope modification method is to improve the performance of the ENO schemes for the solutions which contain contact discontinuities, the numerical experiments we will present in this section are either on linear equations with discontinuous initial values or on the Euler equations for gas dynamics whose solutions contain contact discontinuities. All the examples are standard problems widely used in the literature to test various schemes for the hyperbolic conservation laws.

With these examples, in addition to showing the performance of our method, we also try to give some suggestions on how to choose the parameters in our algorithms since we have not been able to establish any theoretically meaningful rule to determine these parameters.

EXAMPLE 5.1. We apply our method to 1D linear model problem

$$u_t + u_x = 0, \qquad -1 \leqslant x \leqslant 1 \tag{5.1}$$

$$u(x, 0) = u_0(x) \tag{5.2}$$

with periodic boundary condition.

We test our method for this problem with each of the following four initial conditions. Divide the interval $[-1, 1]$ into 100 cells of equal size. The center of the jth cell is $x_j = (j - 50.5)h$, where $h = \frac{1}{50}$. The four initial conditions are

$$v_j^0 = \begin{cases} 1, & 35 \leqslant j \leqslant 65, \\ 0, & \text{otherwise}, \end{cases} \tag{5.3}$$

$$v_j^0 = \begin{cases} (1 - [(j - 50)/15]^2)^{1/2}, & 35 \leqslant j \leqslant 65, \\ 0, & \text{otherwise}, \end{cases} \tag{5.4}$$

$$v_j^0 = e^{-300(x_j - 0.5)^2} \tag{5.5}$$

and

$$v^0_{j+25 \,(\mathrm{mod}\, 100)} = \begin{cases} -y_j \sin(\frac{3}{2}\pi y_j^2), & -1 \leqslant y_j \leqslant -\frac{1}{3}, \\ |\sin(2\pi y_j)|, & |y_j| < \frac{1}{3}, \\ 2y_j - 1 - \sin(3\pi y_j)/6, & \frac{1}{3} < y_j < 1. \end{cases} \tag{5.6}$$

In the last condition, $y_j = x_j - 0.01$. Essentially, the first three conditions are those used by Zalesak [15] (see also the references therein) and the last one is that used by Harten *et al.* [4, 9].

The numerical solutions for the initial condition (5.3) are displayed in Figs. 1–12. In the computations for the Figs. 1–5, the second-order ENO scheme is used. The CFL number is fixed at 0.8 and the SM coefficients α_j's in (3.4) are chosen to be independent of j and n. We increase $\alpha_j \equiv \alpha$ from 0 to 10 and, for each choice of α, run the program twice for 250 time steps and 1250 time steps, respectively. The figures show clearly that, for small α, the discontinuities are smeared more and more as the the number of the time steps increases. However, when the coefficient reach about 1.9–2.3, the smearing appears to be essentially eliminated. This is indicated by the coincidence of the graphs of the numerical solutions obtained by running the program over the two different numbers of time steps. For a given ENO scheme and a fixed CFL number, we call the smallest α which is capable of eliminating the smearing effect the *critical value* of the SM coefficient with respect to the scheme and the CFL number.

Remark 5.1. A quantity equal to or slightly larger than the supremum of the critical value over the range $[0, 1]$ of the CFL number is a good candidate for the choice of the SM coefficient. For the solutions which lack smooth structure we can choose a larger SM coefficient. Otherwise, we should choose one near or equal to the supremum of the critical value.

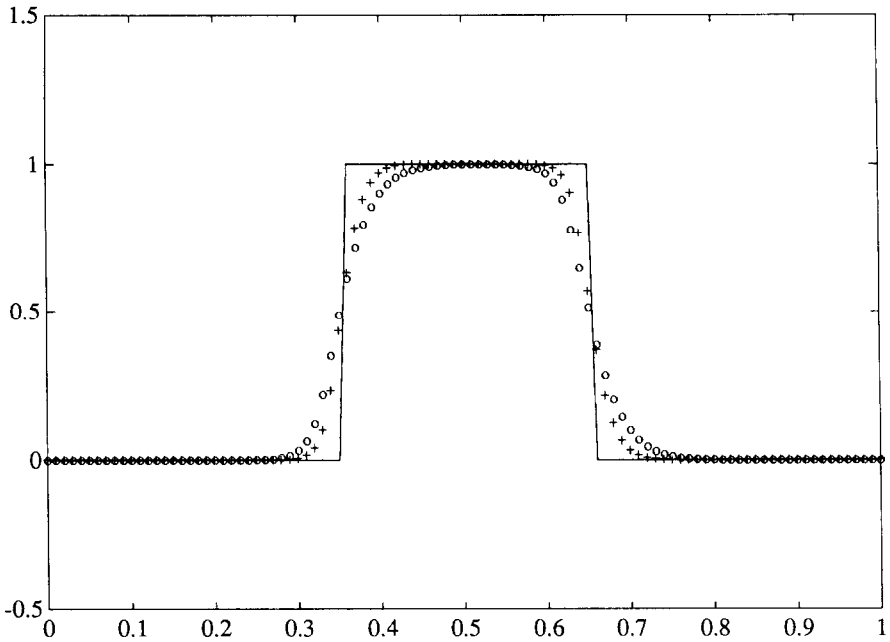

FIG. 1. Linear square wave: +: 250 steps; ∘: 1250 steps; order: 2—1; constant alfa = 0.0, CFL = 0.8.

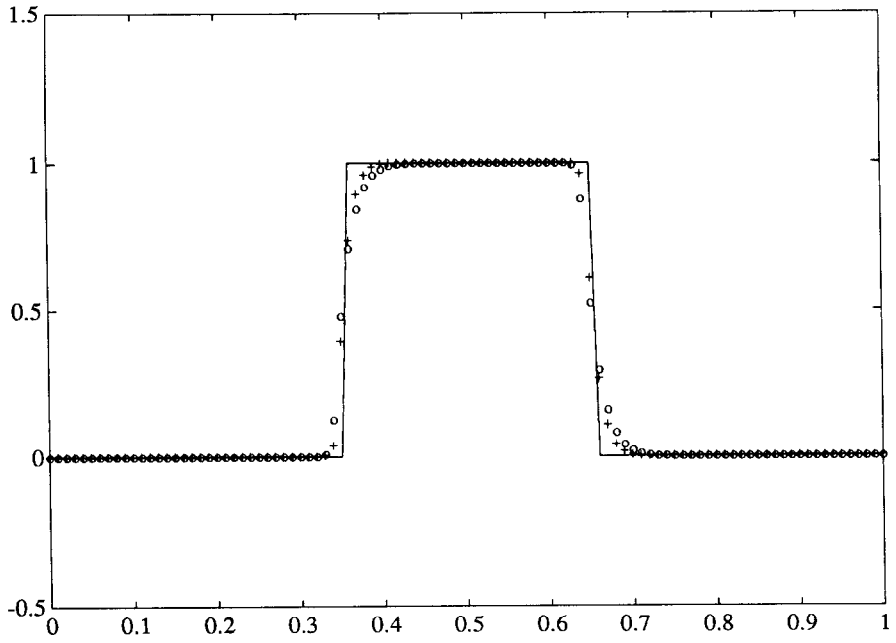

FIG. 2. Linear square wave: +: 250 steps; ∘: 1250 steps; order: 2—1; constant alfa = 1.5, CFL = 0.8.

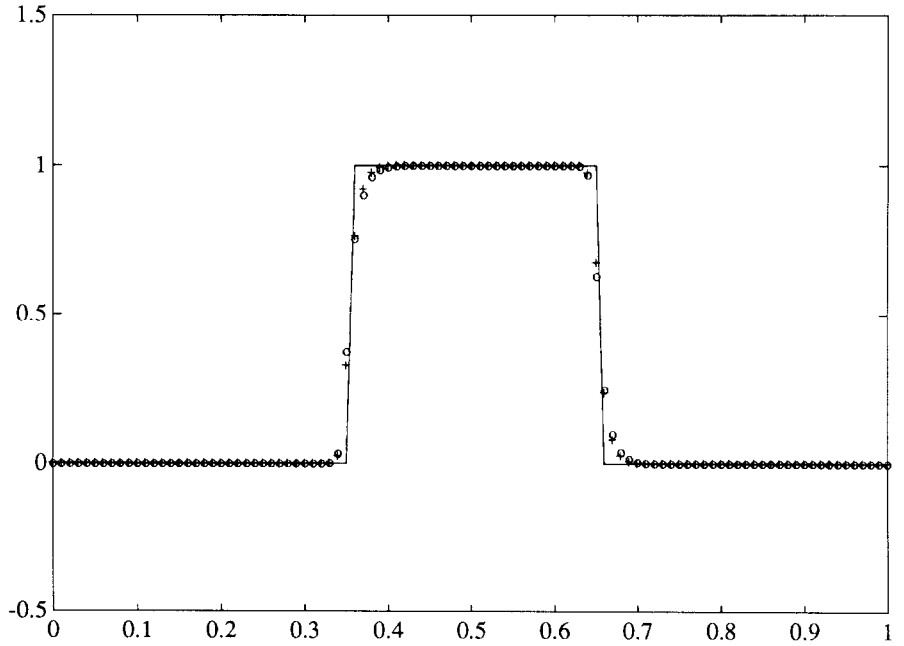

FIG. 3. Linear square wave: +: 250 steps; ∘: 1250 steps; order: 2—1; constant alfa = 1.9, CFL = 0.8.

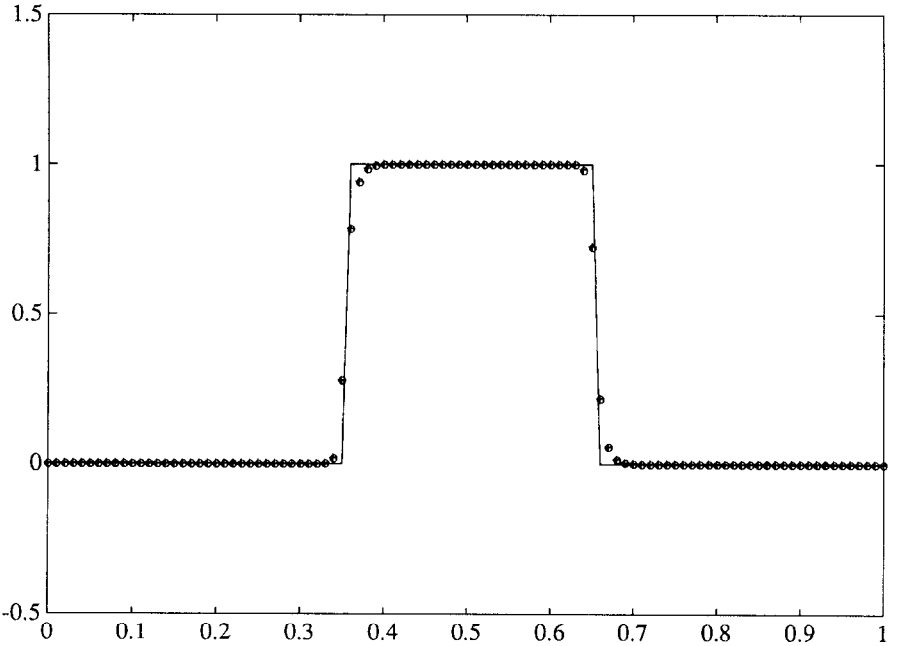

FIG. 4. Linear square wave: +: 250 steps; ∘: 1250 steps; order: 2—1; constant alfa = 2.3, CFL = 0.8.

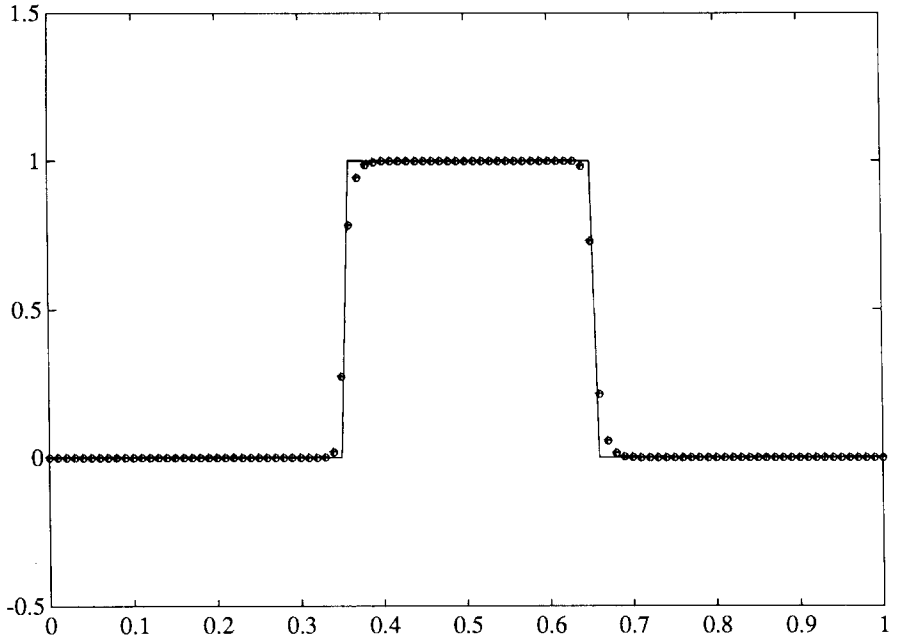

FIG. 5. Linear square wave: +: 250 steps; ∘: 1250 steps; order: 2—1; constant alfa = 10.0, CFL = 0.8.

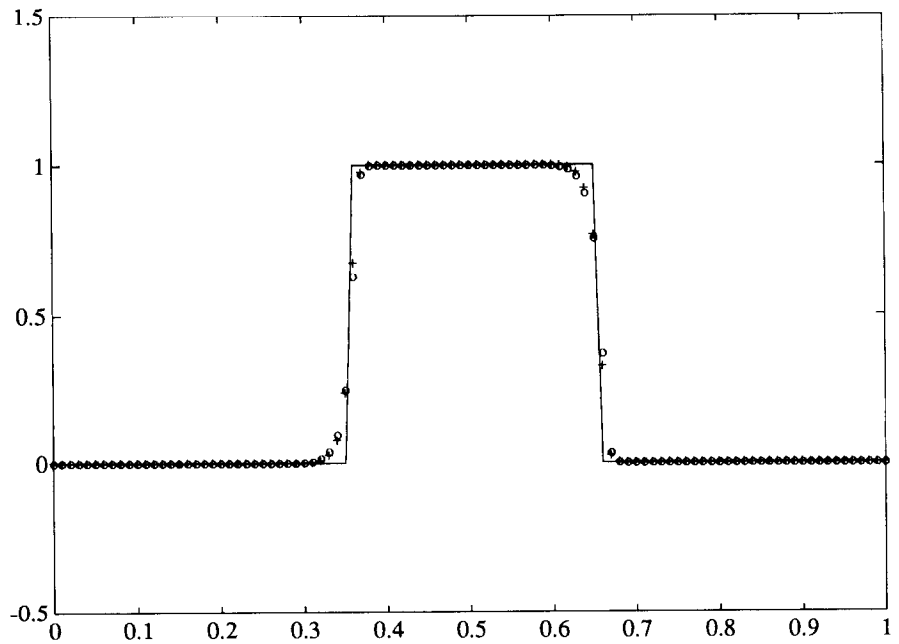

FIG. 6. Linear square wave: +: 250 steps; ∘: 1250 steps; order: 2—1; constant alfa = 1.9, CFL = 0.2.

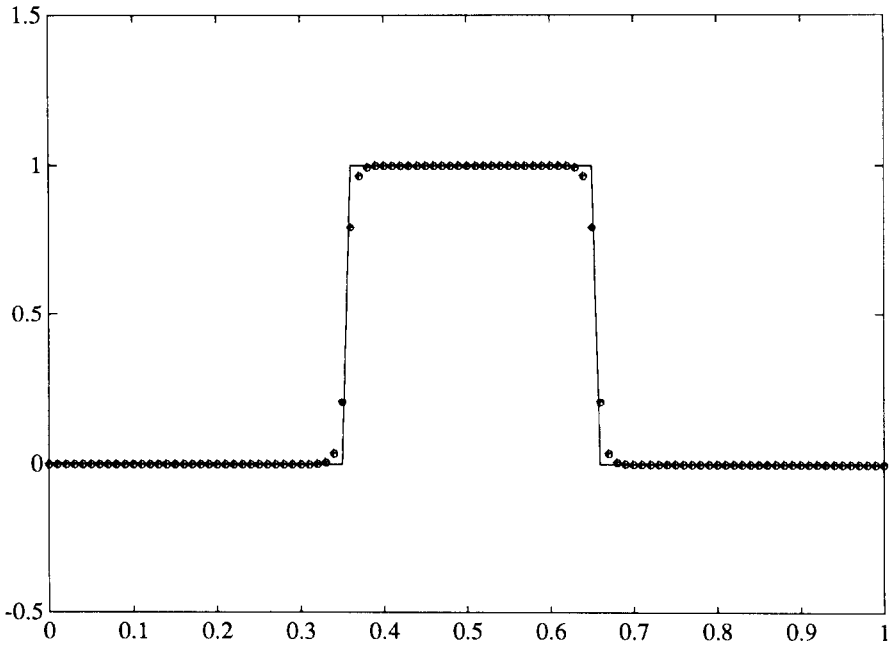

FIG. 7. Linear square wave: + : 250 steps; ∘ : 1250 steps; order: 2—1; constant alfa = 1.9, CFL = 0.5.

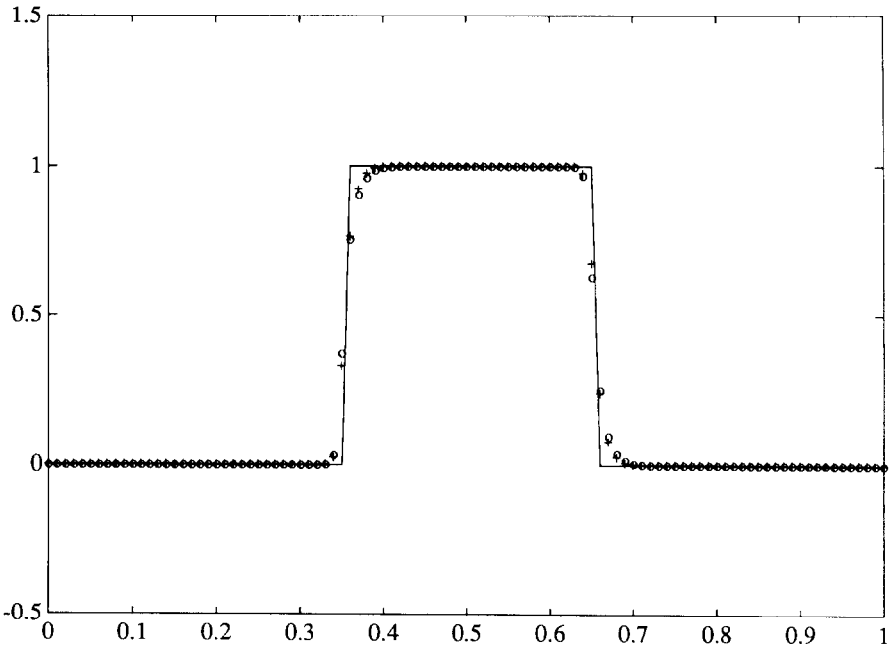

FIG. 8. Linear square wave: + : 250 steps; ∘ : 1250 steps; order: 2—1; constant alfa = 1.9, CFL = 0.8.

Remark 5.2. For the solution-dependent SM coefficient (3.21), one can similarly "define" the critical value for the parameter c. The recommendations in the last remark also applies here.

Figures 6–8 show the effect of CFL numbers on the critical values. We do the same computations as for the Figs. 1–5 with different CFL numbers. The SM coefficients are $\alpha = 1.9$ and $\alpha = 2.3$. We found that the effect is minor.

Notice that although the CFL numbers have little effect on the critical value of the SM coefficients, they do play a role in the profiles of the solutions over the linear discontinuities. The sharpening effect is not well balanced, i.e., the steepness at the heads of the discontinuities is different from that at the tails when the CFL numbers are far away from ± 0.5. Looking at the Fig. 1 carefully, one sees that this property of nonsymmetry already exists with the original ENO schemes.

For solutions with rich smooth structures and/or for multi-dimensional problems, when our slope modification method is applied and the resulting program is run for a huge number of time steps, this phenomenon becomes more serious. To overcome this trouble, observe that at the head of a discontinuity, $|(\Delta_{j-1}v)/\Delta_j v|$ is very large, while at the tail, it is very small. We hence define the following balance operator

$$\beta_j(\lambda_j, b) = \left| \frac{\Delta_{j-1} v}{\Delta_j v} \right|^{b(\lambda_j - 0.5\,\mathrm{sgn}(\lambda_j))}, \tag{5.7}$$

where b is a positive parameter to be chosen, $\lambda_j = \bar{a}_j(\tau/h)$ is the local CFL number, and $\bar{a}_j$ is the characteristic speed. We will see the effect of this operator in the examples displayed in the Figs. 17–20.

Figures 8–12 show the effect of the order of accuracy on the the critical values of the SM coefficients. In these figures, $r-0$ denotes the "rth order" ENO schemes, while $r-1$ denotes the rth order ENO schemes, both in the sense of [4]. We find that the effect is also minor. This is interesting since the jumps of a higher order reconstruction at the cell interfaces over the transitions of the discontinuities are much smaller than those of a lower order reconstruction (see, again, the figures at the end of [4]).

The fact that the critical value of the SM coefficients is relatively independent of, rather than inversely proportional to, the jumps for different orders of the schemes is consistent to the fact that the higher order ENO schemes smear the contact discontinuities less than the lower order ones do.

The results for the initial condition (5.4) are displayed in the Figs. 13–20. In Figs. 13–16, we use the SM coefficient 1.9. The improvement is apparent. The Figs. 17–20 test the effect of the balance operator (5.7). This time we run our program of the second-order ENO for 6000 time steps. For the Figs. 17 and 18, we use the constant SM coefficients 1.9 with the balance operators $b = 4.3$ and $b = 0$, respectively. For the Figs. 19 and 20, we use (3.21) with $c = 33$ accompanied by the balance operators $b = 4.3$ and $b = 0$, respectively.

Figures 21–22 display the numerical results for initial condition (5.5); Figs. 23–24

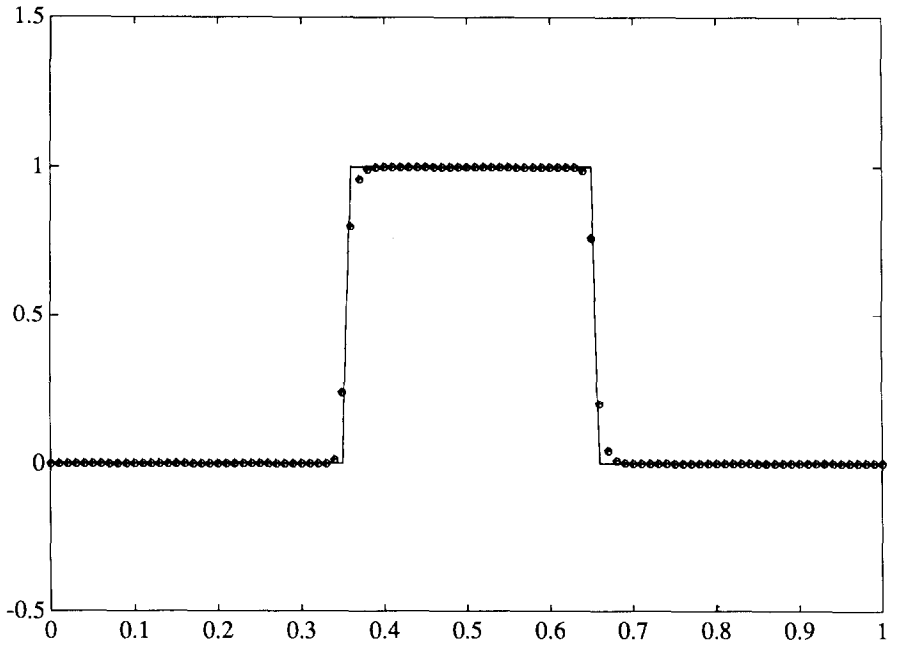

FIG. 9. Linear square wave: + : 250 steps; ∘ : 1250 steps; order: 3—0; constant alfa = 1.9, CFL = 0.8.

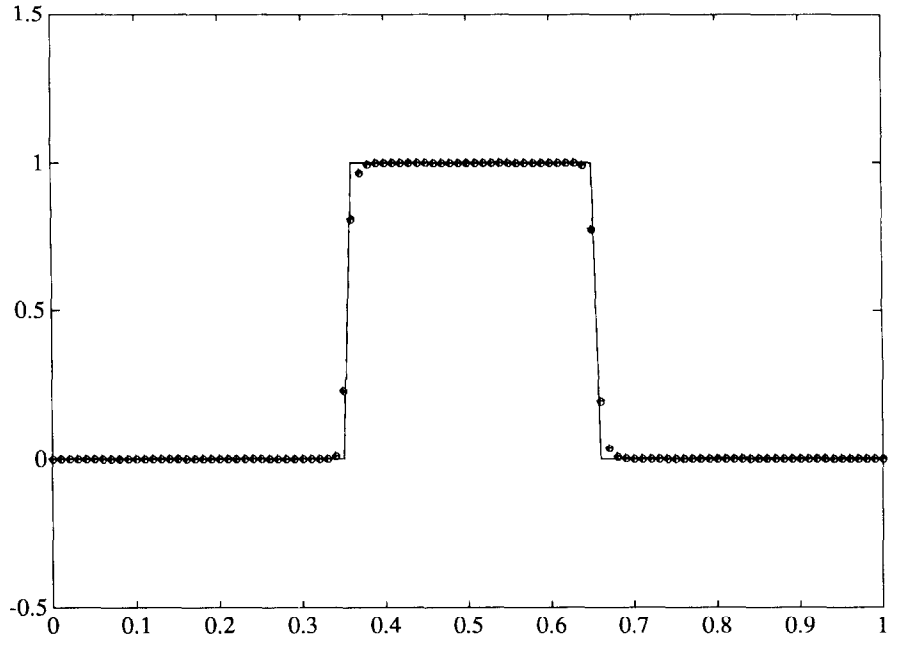

FIG. 10. Linear square wave: + : 250 steps; ∘ : 1250 steps; order: 3—1; constant alfa = 1.9, CFL = 0.8.

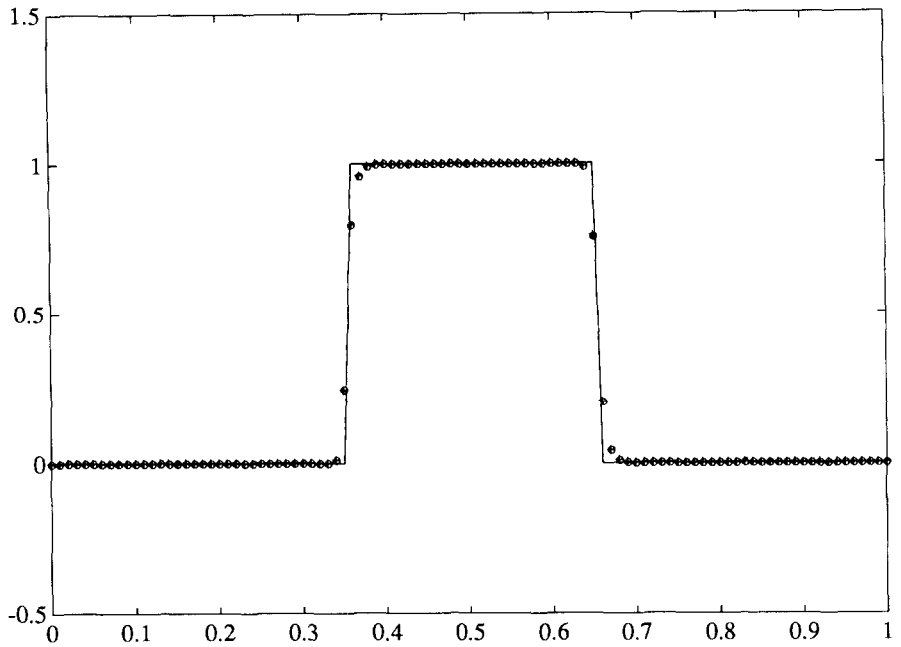

FIG. 11. Linear square wave: + : 250 steps; ∘ : 1250 steps; order: 4—0; constant alfa = 1.9, CFL = 0.8.

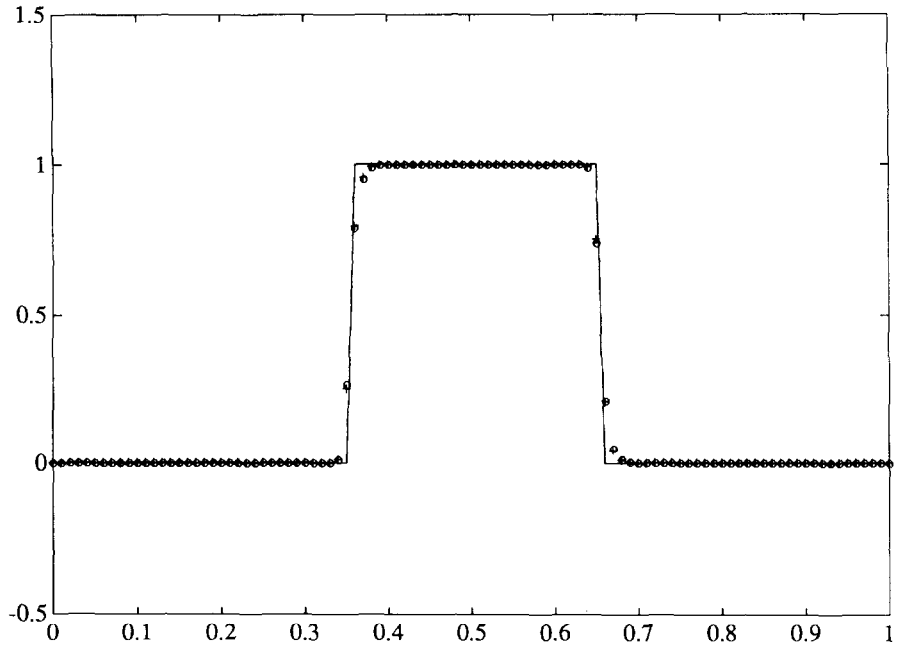

FIG. 12. Linear square wave: + : 250 steps; ∘ : 1250 steps; order: 4—1; constant alfa = 1.9, CFL = 0.8.

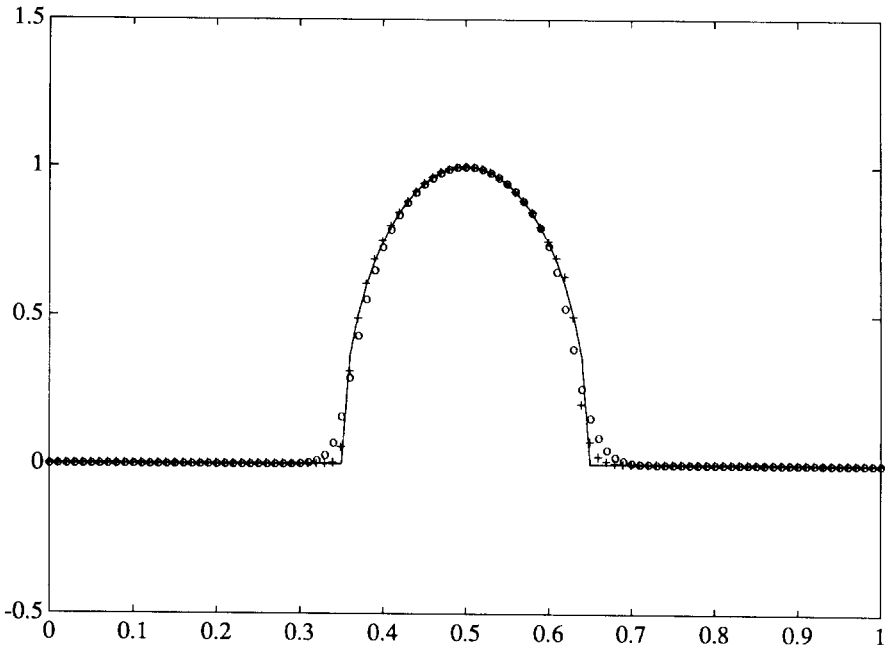

FIG. 13. Linear, semi-circle wave: +: with ACM; ∘: without ACM; order: 2—1; time steps = 250, CFL = 0.8.

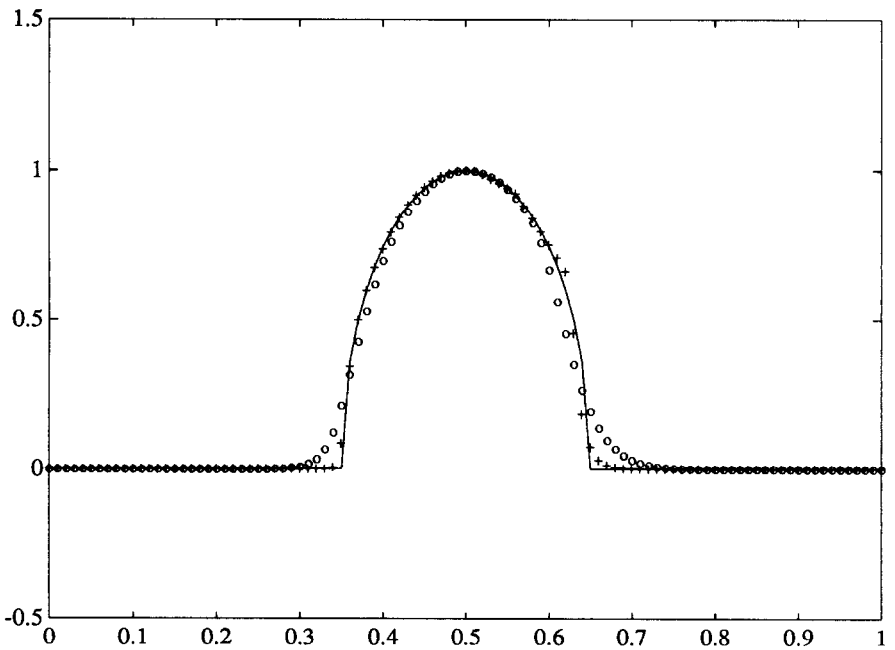

FIG. 14. Linear, semi-circle wave: +: with ACM; ∘: without ACM; order: 2—1; time steps = 1250, CFL = 0.8.

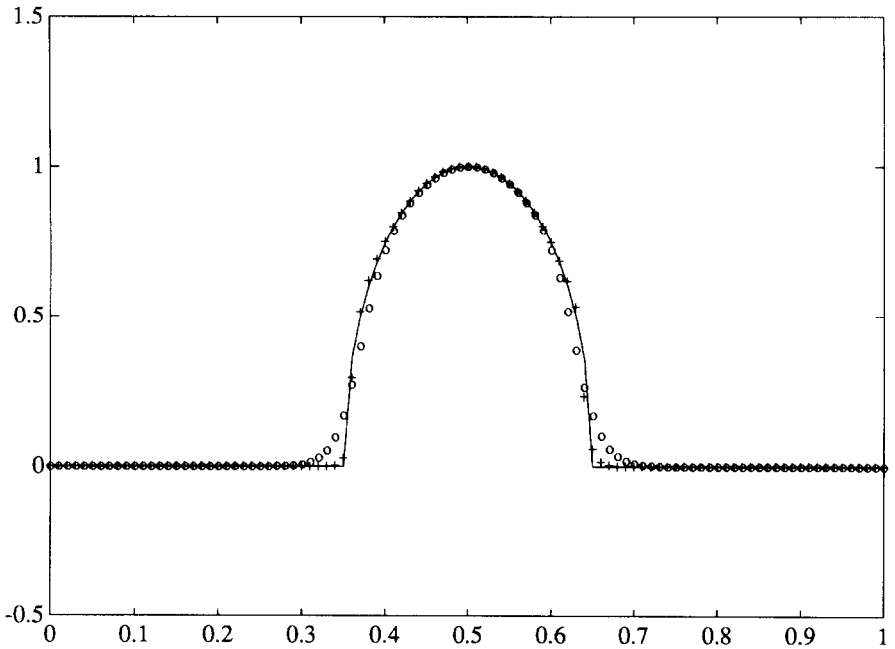

FIG. 15. Linear, semi-circle wave: + : with ACM; ∘ : without ACM; order: 3—1; time steps = 1250, CFL = 0.8.

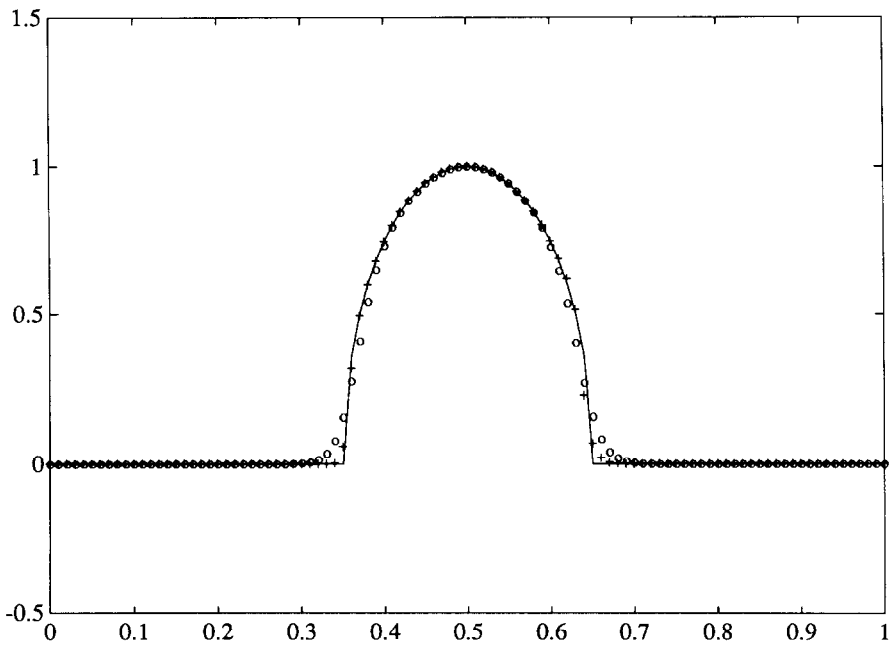

FIG. 16. Linear, semi-circle wave: + : with ACM; ∘ : without ACM; order: 4—1; time steps = 1250, CFL = 0.8.

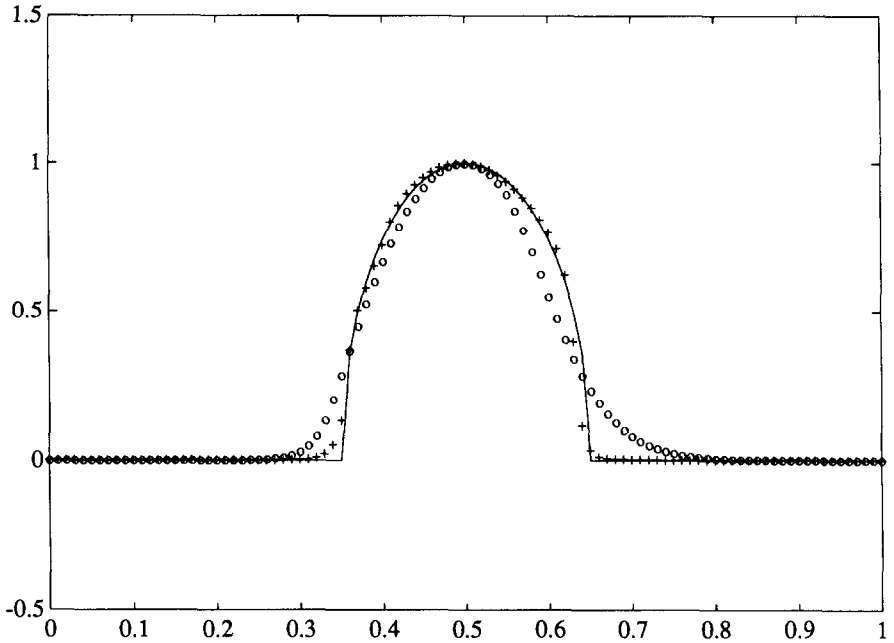

FIG. 17. Linear, semi-circle wave: +: with ACM; ∘: without ACM; order: 2—1; time steps = 6000, CFL = 0.8.

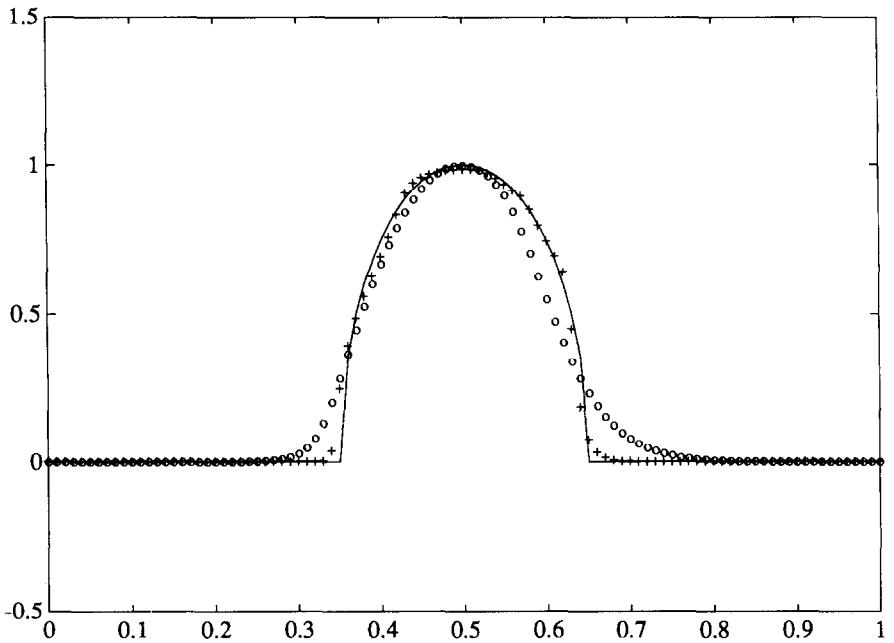

FIG. 18. Linear, semi-circle wave: +: with ACM; ∘: without ACM; order: 2—1; time steps = 6000, CFL = 0.8.

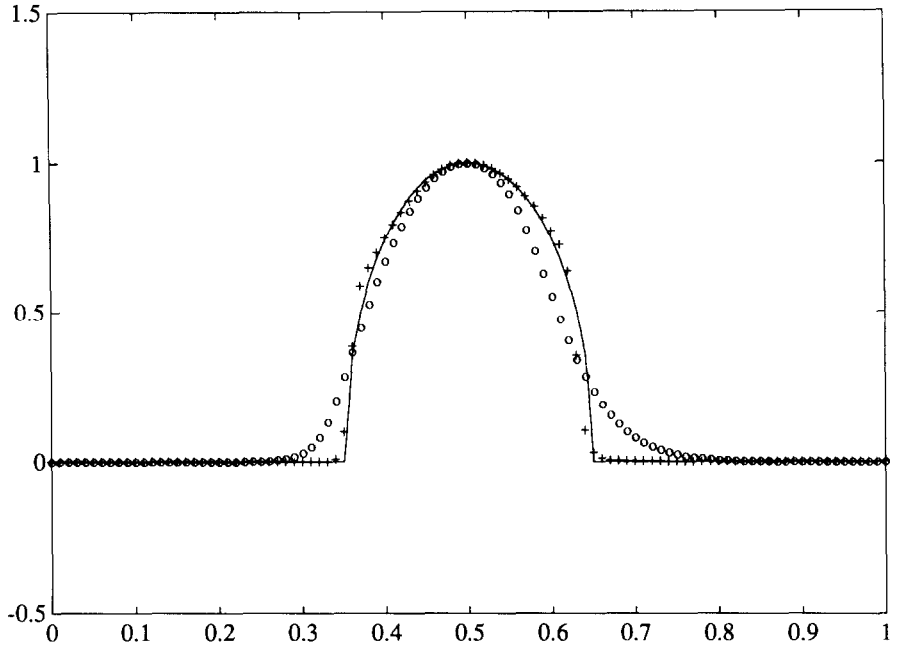

FIG. 19. Linear, semi-circle wave: + : with ACM; ∘ : without ACM; order: 2—1; time steps = 6000, CFL = 0.8.

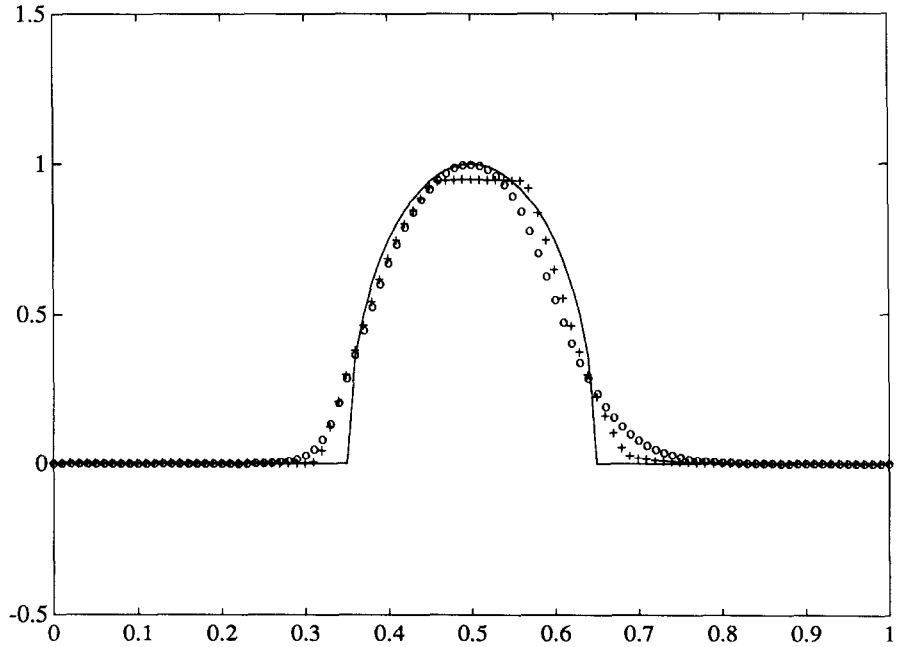

FIG. 20. Linear, semi-circle wave: + : with ACM; ∘ : without ACM; order: 2—1; time steps = 6000, CFL = 0.8.

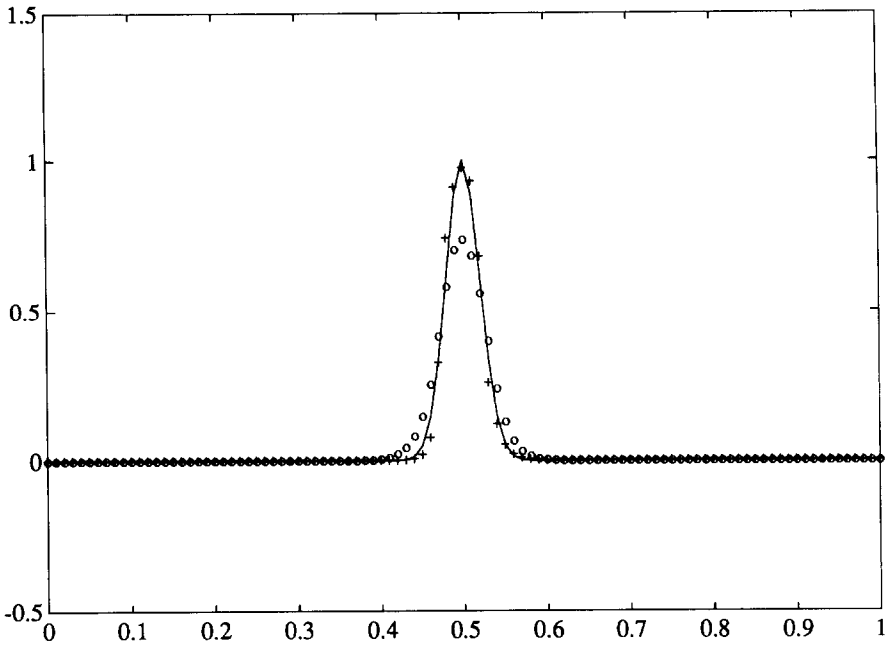

FIG. 21. +: with ACM; ∘: without ACM; order: 3—0; time steps = 600, CFL = 0.1.

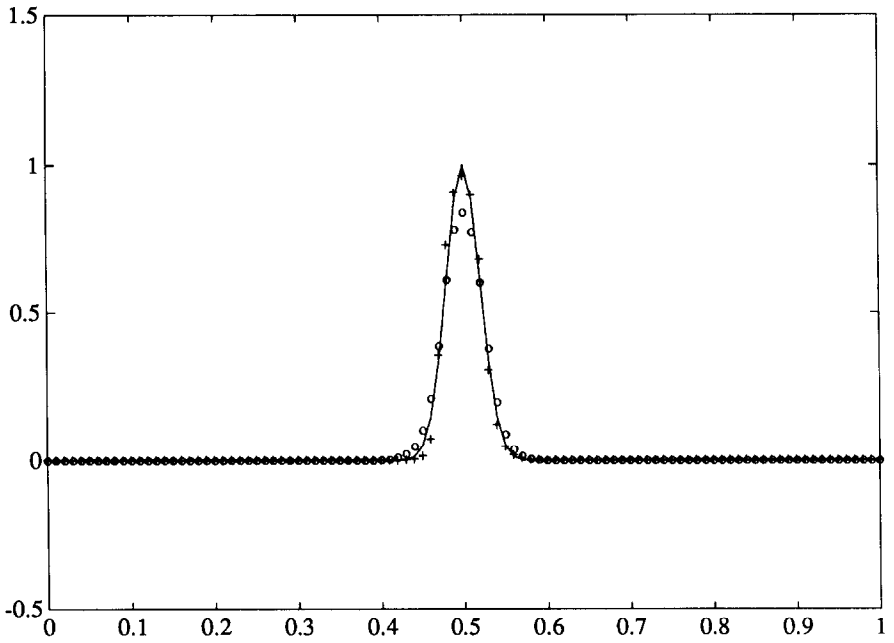

FIG. 22. +: with ACM; ∘: without ACM; order: 4—0; time steps = 600, CFL = 0.1.

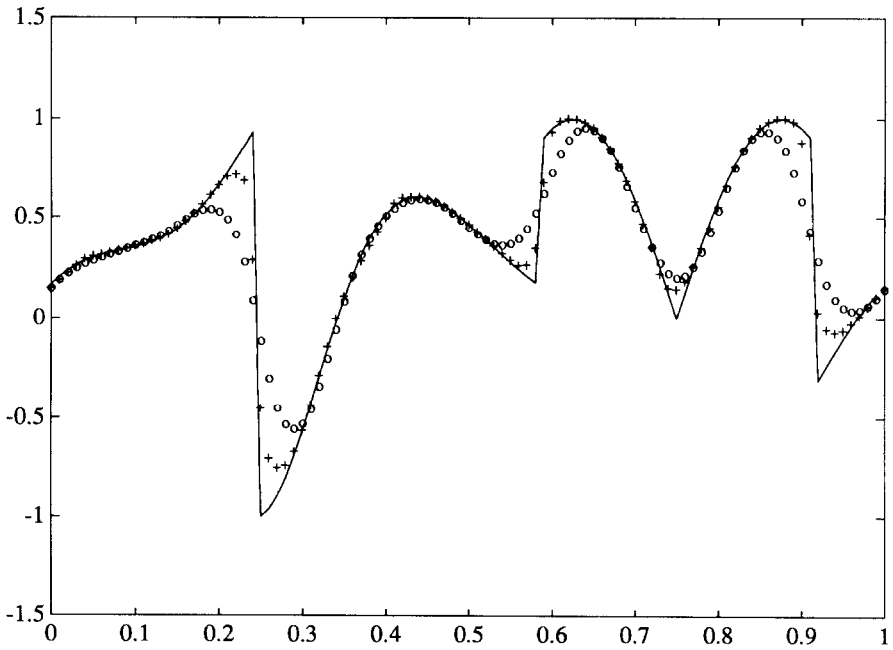

FIG. 23. +: with ACM; ∘: without ACM; order: 3—0; time steps = 1000, CFL = 0.8.

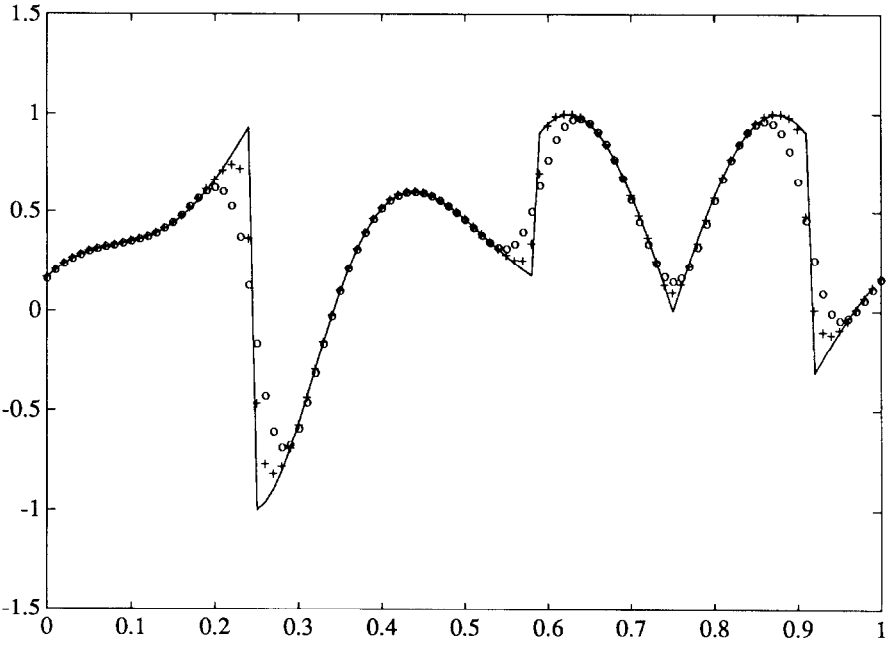

FIG. 24. +: with ACM; ∘: without ACM; order: 4—0; time steps = 1000, CFL = 0.8.

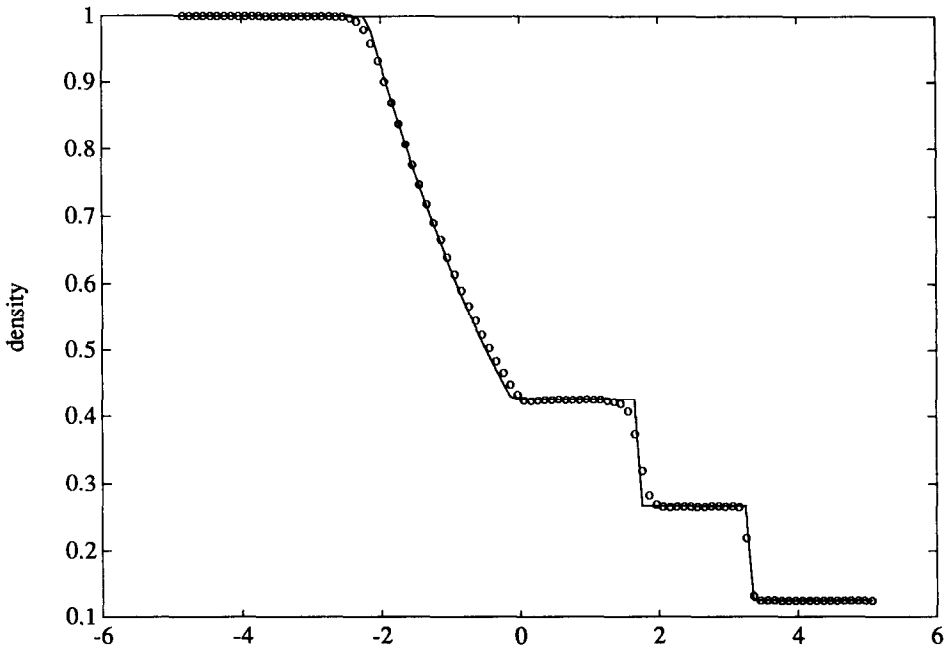

FIG. 25. Sod problem, "(fourth-) order" ENO without SM.

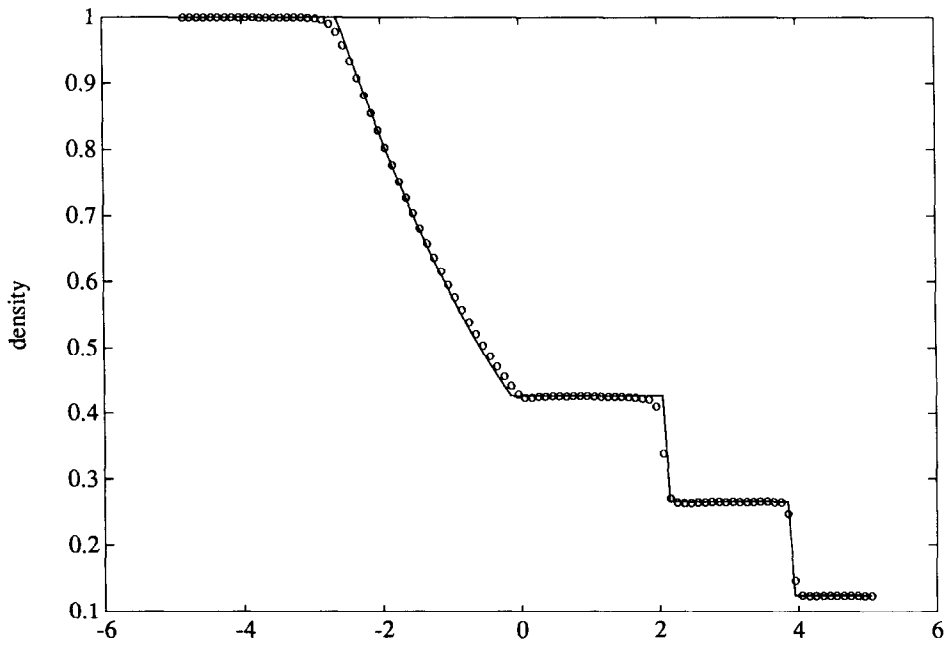

FIG. 26. Sod problem, "(fourth-) order" ENO with SM.

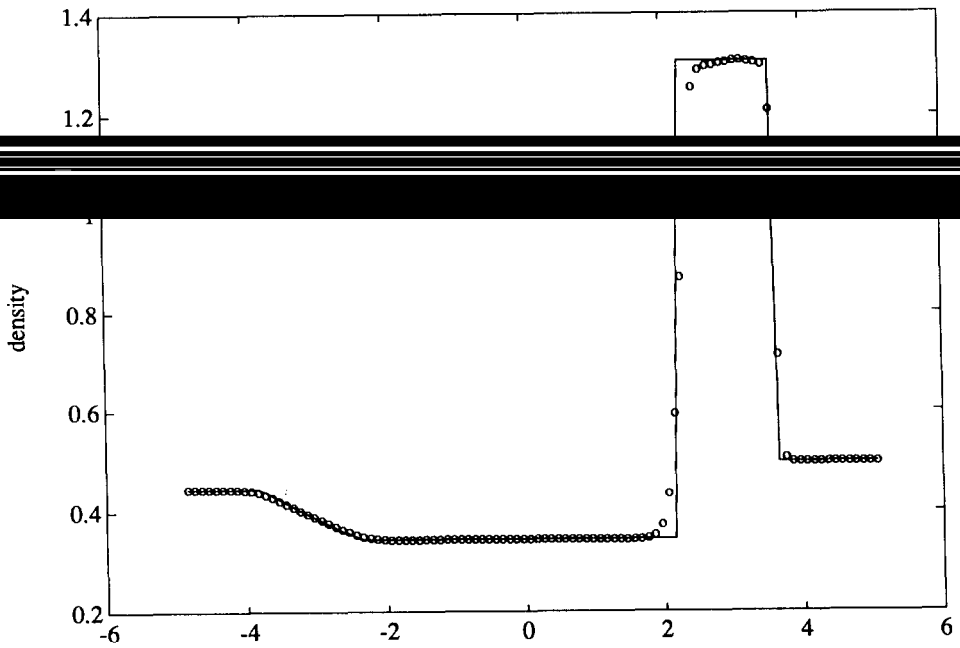

FIG. 27. Lax problem, "(fourth-) order" ENO without SM.

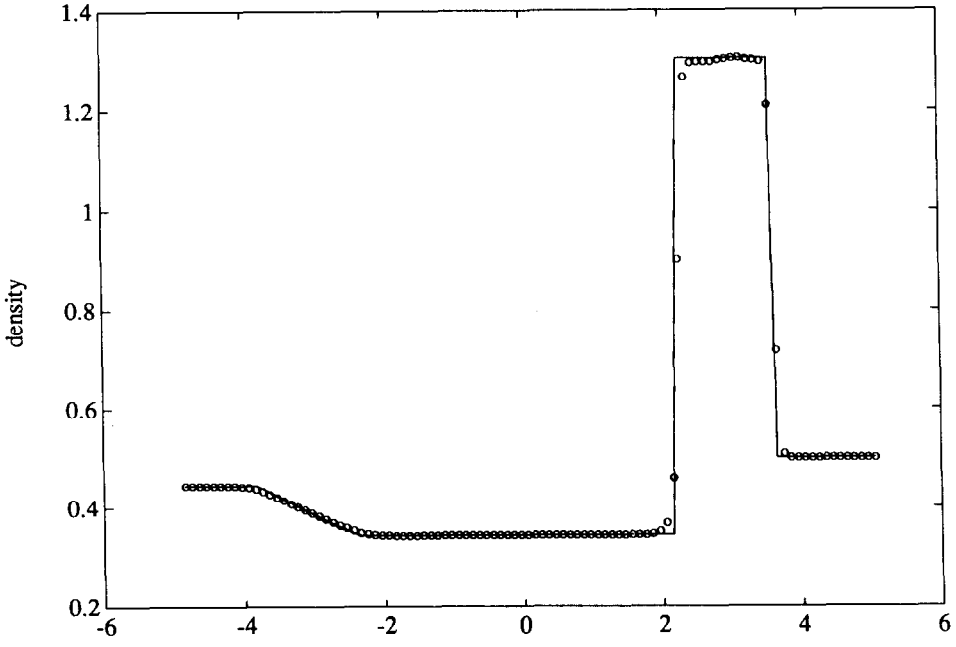

FIG. 28. Lax problem, "(fourth-) order" ENO with SM.

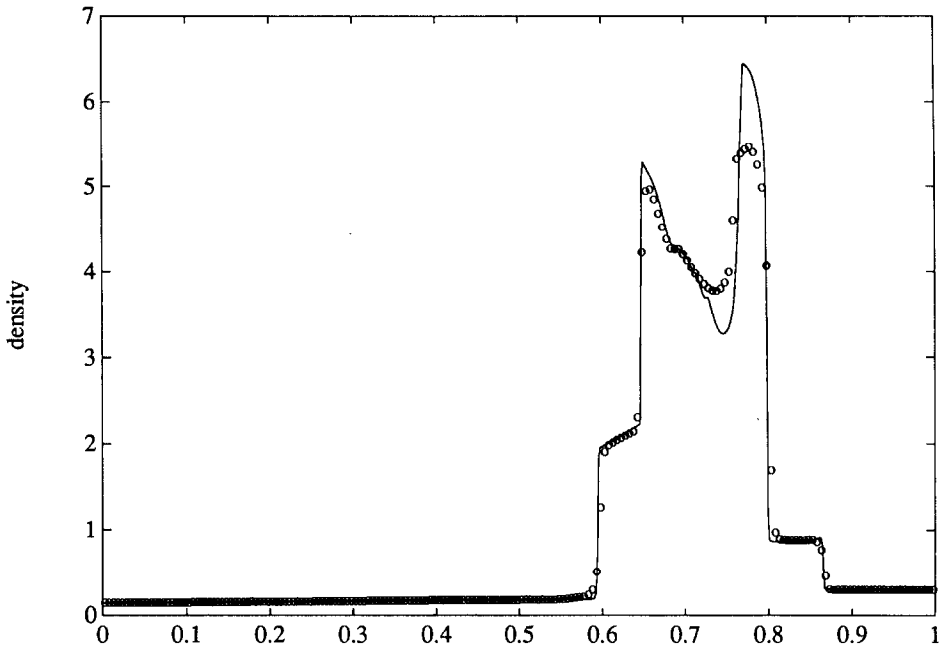

FIG. 29. Blast waves, second-order ENO with SM, $t = 0.038$.

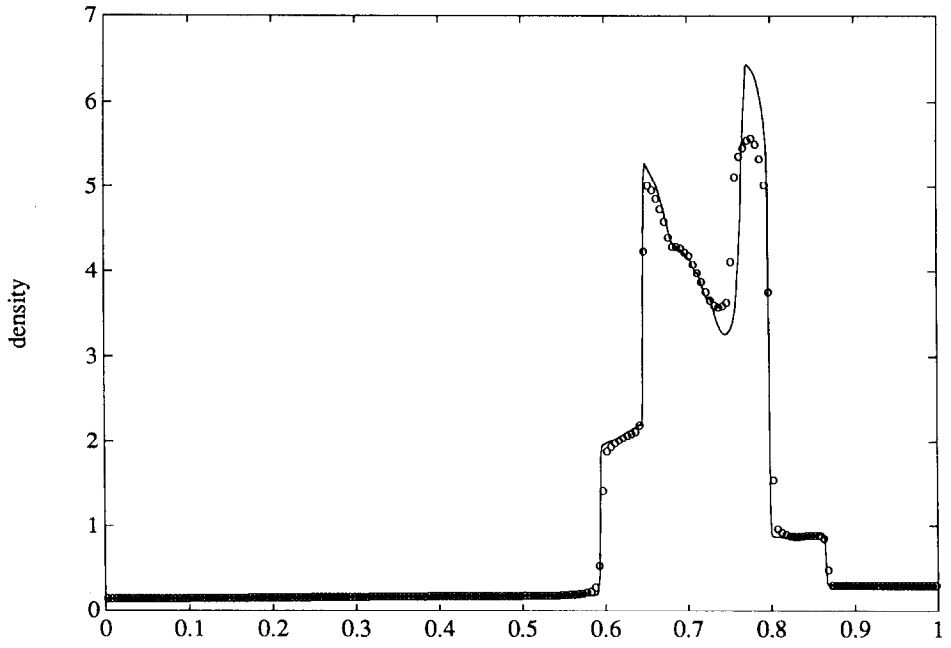

FIG. 30. Blast wave, fourth-order ENO with SM, $t = 0.038$.

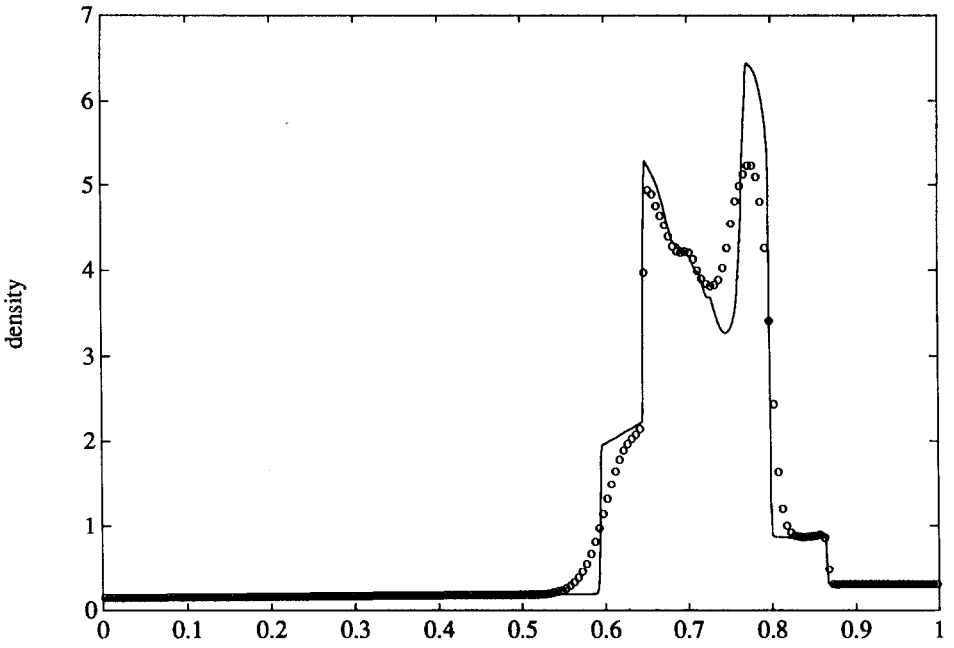

FIG. 31. Blast wave, fourth-order ENO without SM, $t = 0.038$.

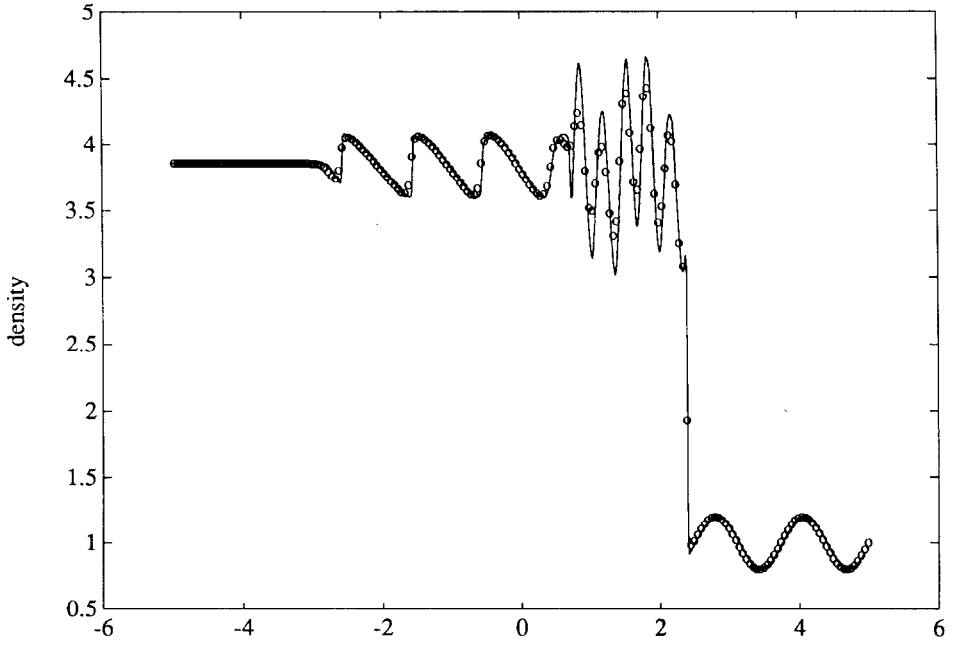

FIG. 32. Shock/turbulence, fourth-order ENO with SM.

The results at $t = 0.038$ are displayed in Figs. 29, 30, and 31. The solid lines are the numerical solutions obtained by the second-order ENO scheme and the slope modification method with 800 cells. Figure 29 is the result of the second-order ENO scheme with Algorithm 4.2 and Fig. 30 is the result of the fourth-order ENO schemes with Algorithm 4.1. For comparison, in Fig. 31 we display the numerical result of the fourth-order ENO without the slope modification. Notice that all the contact discontinuities are well captured by the ENO schemes with our method. For the computations with 200 space cells, even the very delicate contact discontinuity mentioned above occupies only 1–2 transition points. These results are obviously better than those obtained by the two versions of the PPM schemes–the PPMDE and the PPMLR (see [14]) whose results are already very good. Unfortunately, we have not been able to keep this narrow transition when we refine the grid. Finally, we can see that the two algorithms perform equally well.

EXAMPLE 5.4. To see the performance of our method for the problems that have some structure, we apply it to the Euler equations (4.1) with the following initial condition:

$$(\rho, q, P) = \begin{cases} (3.857143, 2.629369, 10.33333), & x < -4 \\ (1 + 0.1 \sin 5x, 0, 1), & x \geqslant -4. \end{cases} \tag{5.12}$$

This is a model problem for shock/turbulence interaction. See [12] for a linearized analysis of this problem, and [7] for a numerical result. We apply our slope modification method with the balance operator on the "fourth-order" ENO schemes. The results are demonstrated in Figs. 32–35. The computations are performed with the CFL number 0.8. The solid line is the result with 800 cells. Comparing the result with that in [7] we can regard it as the exact solution. The circles in Figs. 32 and 33 are the results computed with 200 cells and 400 cells, respectively. For comparison, Figs. 34 and 35 show the results computed with 200 cells and 400 cells, respectively, without the slope modification.

EXAMPLE 5.5. This is a preliminary result for 2D computations. Consider the 2D model problem

$$u_t + u_x + u_y = 0, \qquad (x, y; t) \in \mathbf{R}^2 \times [0, \infty). \tag{5.13}$$

The initial value $u_0(x, y)$ is a periodic function with the period 2 in both x and y. In the region $\Omega = -1 \leqslant x, y \leqslant 1$,

$$u_0(x, y) = \begin{cases} 1, & \text{if } |x - y| \leqslant \sqrt{2}/2, |x + y| \leqslant \sqrt{2}/2, \\ 0, & \text{otherwise.} \end{cases} \tag{5.14}$$

In [10], Harten used this problem to test the performance of the ENO schemes with the 2D reconstructions via deconvolution. Now, we use the reconstructions via primitive functions dimension by dimension and, at the same time, apply the scalar

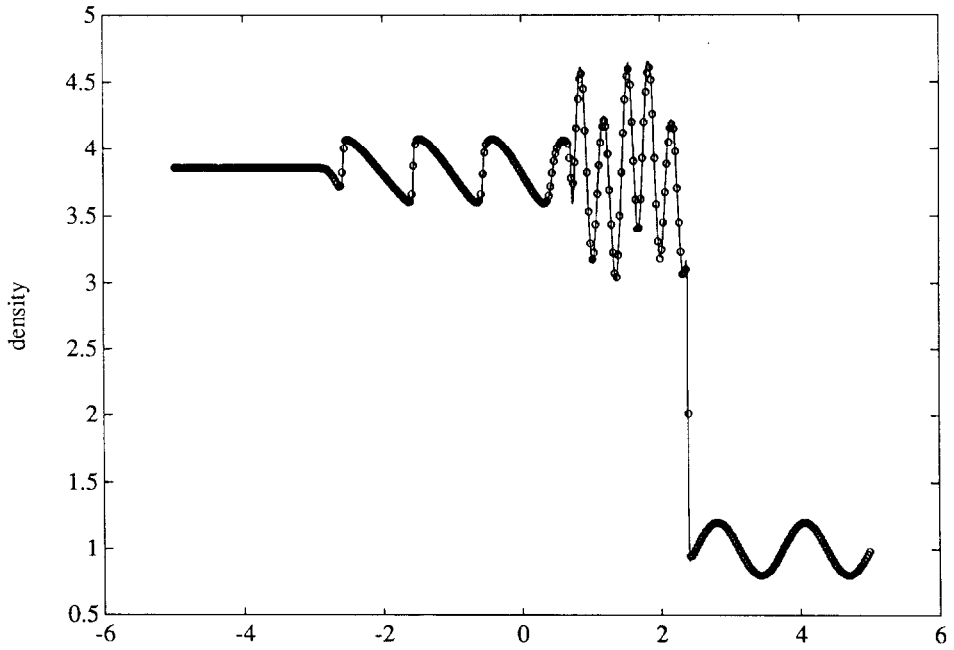

FIG. 33. Shock/turbulence, fourth-order ENO with SM.

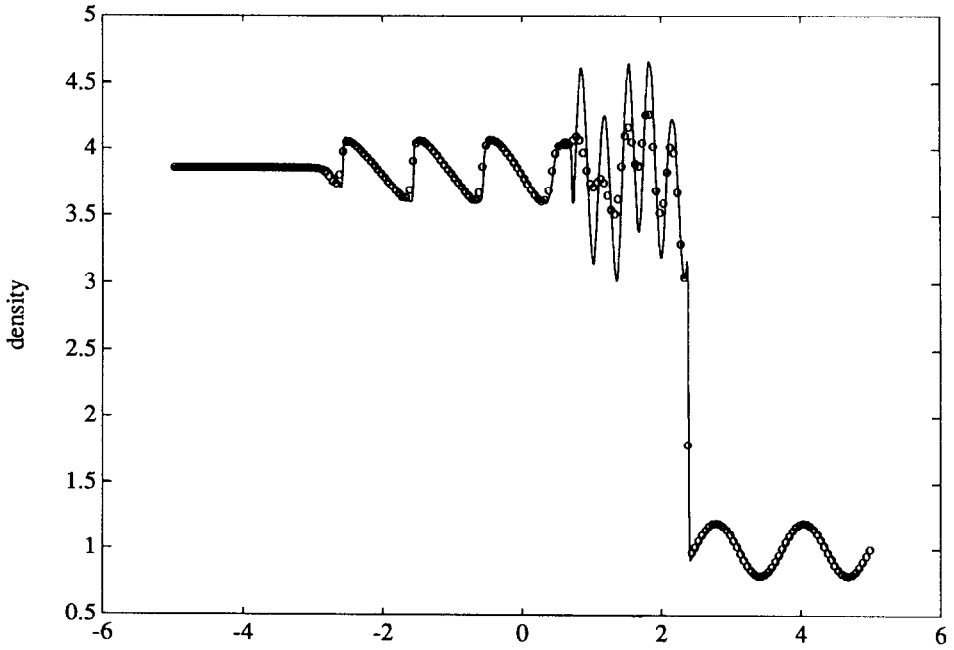

FIG. 34. Shock/turbulence, fourth-order ENO without SM.

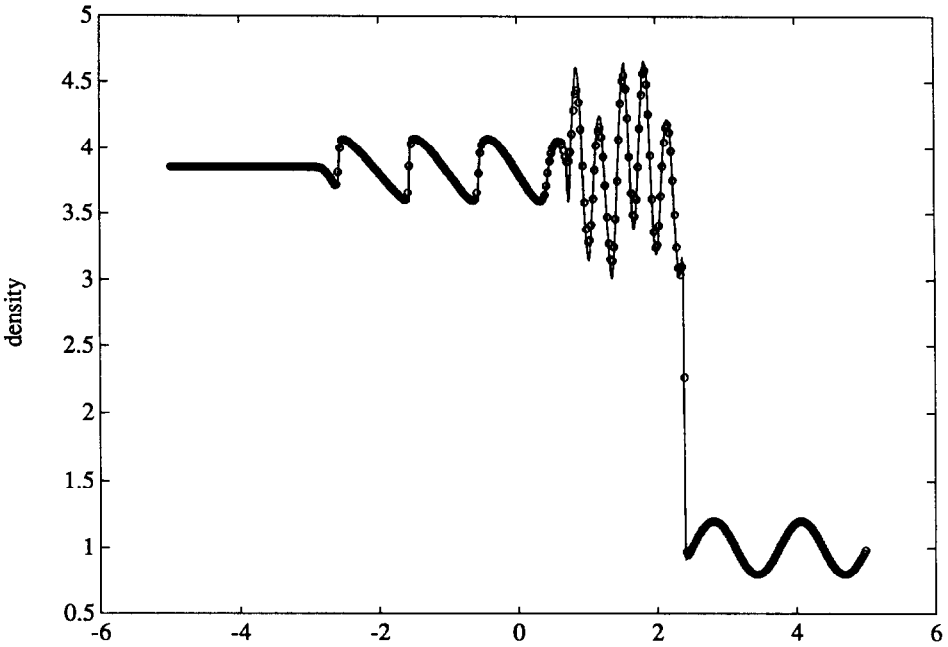

FIG. 35. Shock/turbulence, fourth-order ENO without SM.

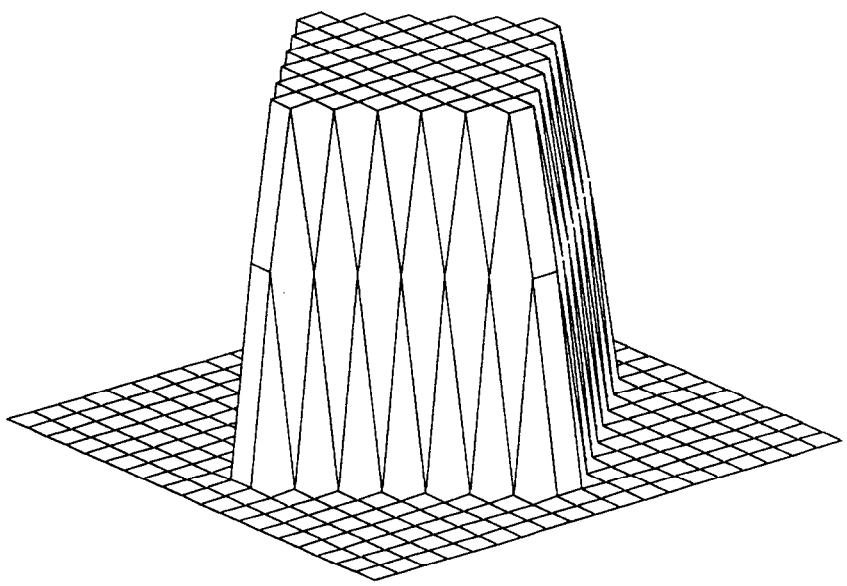

FIG. 36. Exact solution.

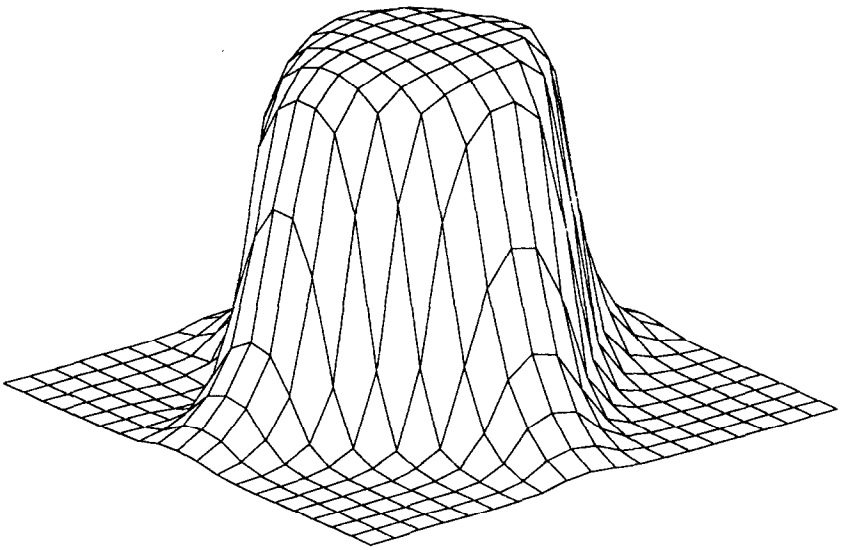

FIG. 37. Second-order ENO, with artificial compression.

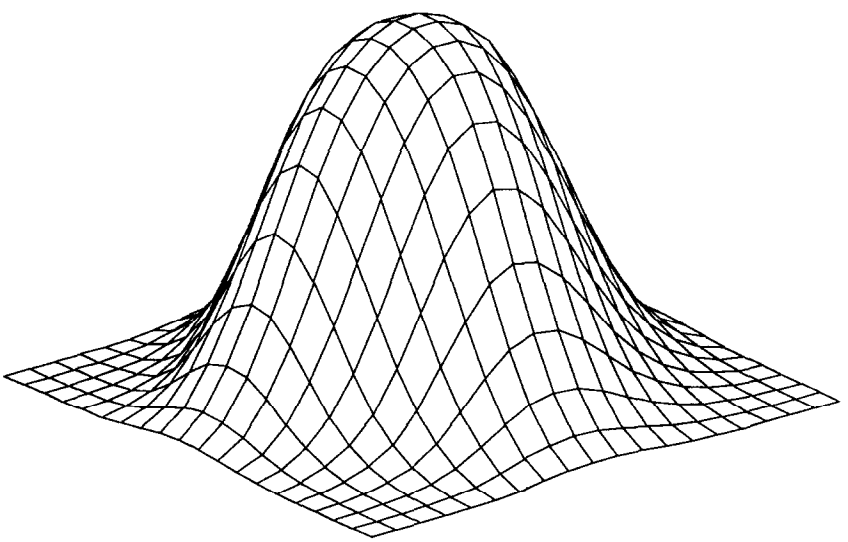

FIG. 38. Second-order ENO, without artificial compression.

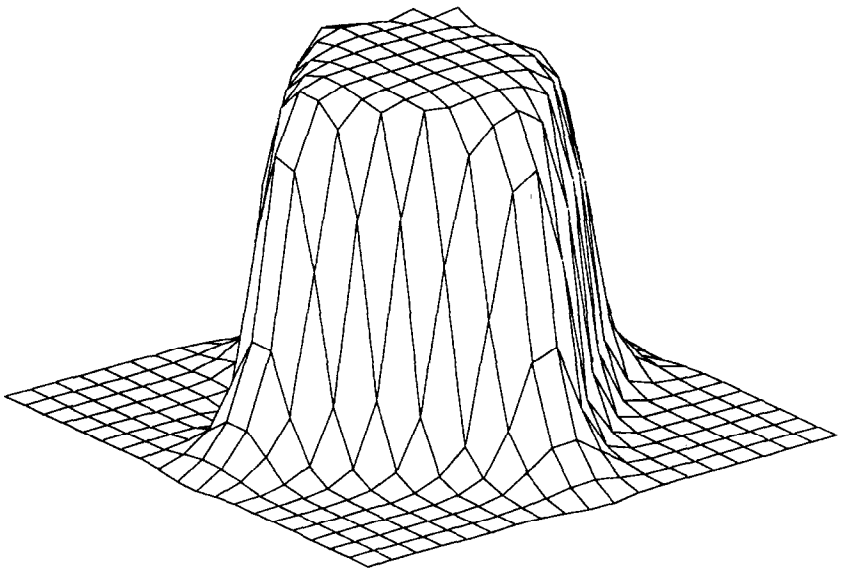

FIG. 39. Third-order ENO, with artificial compression.

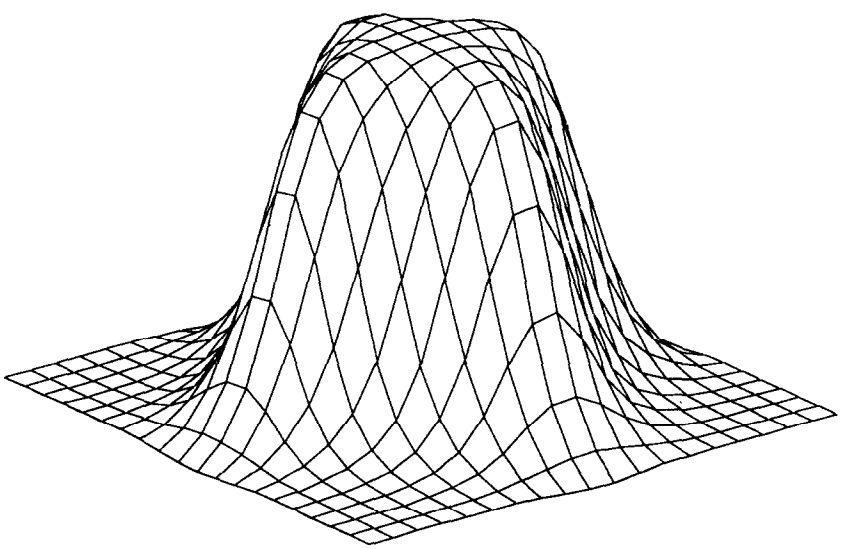

FIG. 40. Third-order ENO, without artificial compression.

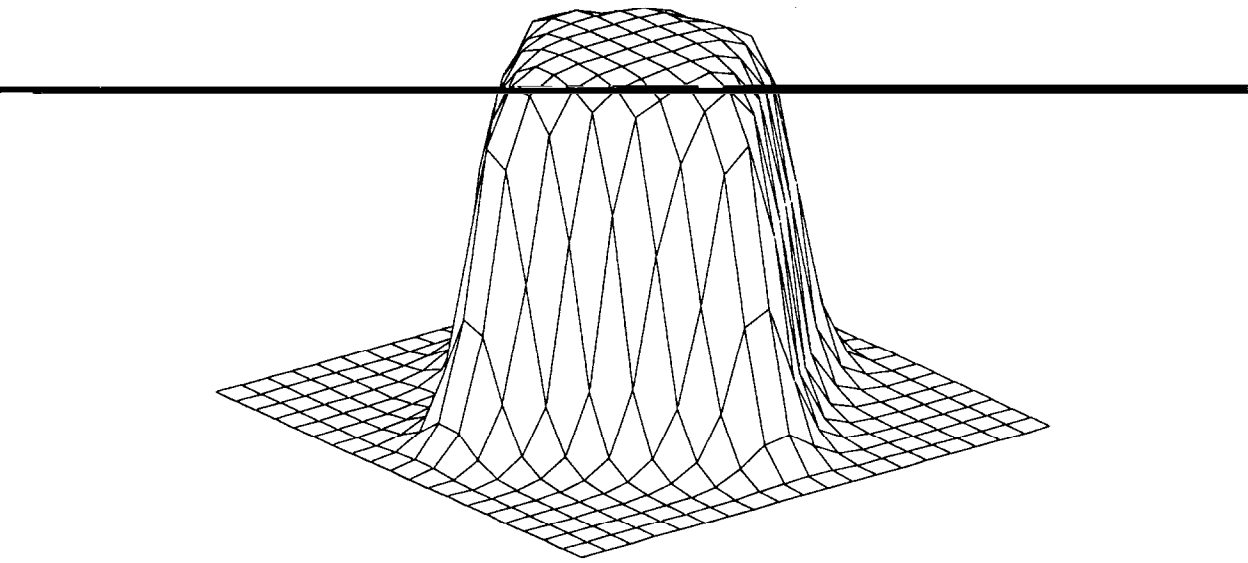

FIG. 41. Fourth-order ENO, with artificial compression.

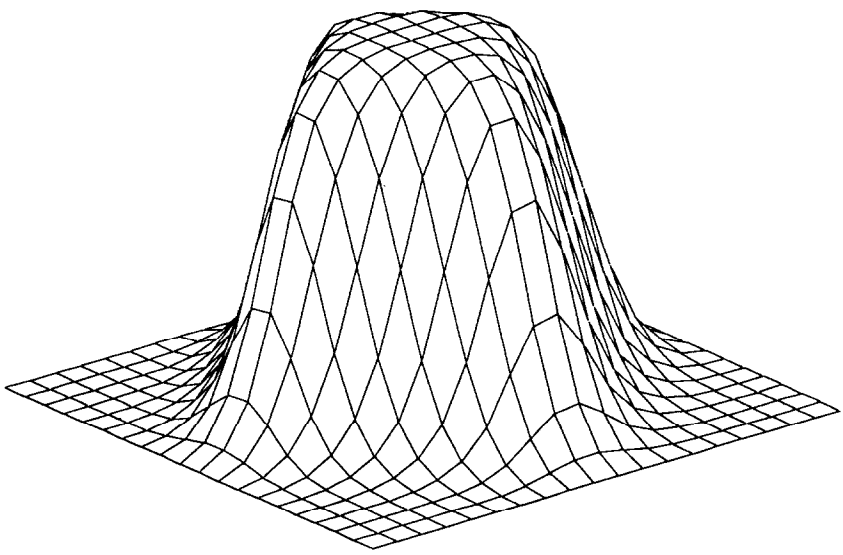

FIG. 42. Fourth-order ENO, without artificial compression.

slope modification algorithm with the balance operator. The CFL number is 0.8×0.8. The computations are performed with 20×20 cells per period. The exact solution in Ω and at $t = 16$, i.e., $n = 200$ time steps and the numerical results in Ω and at the same time with the slope modification applied to the second-, third-, and fourth-order ENO schemes are displayed in the Figs. 36, 37, 39, and 41 respectively, while those without in the Figures 38, 40, and 42, respectively. The apparent improvements shown in these results and the results in [7] indicate that the present method is promising in 2D computations.

ACKNOWLEDGMENTS

I would like to express my highest appreciation for Professor S. Osher's invaluable guidance, encouragement, and support throughout the period of this work. I am also extremely grateful to Professor A. Harten for many helpful discussions and instructions. Thanks also to C.-W. Shu, W. E. D. Mao, and R. Donat for helpful discussions and/or pointing out the errors in the manuscript. Special thanks also to the referee who has carefully read the manuscript and has offered many expert comments, suggestions, and corrections.

REFERENCES

1. A. HARTEN, *Math. Comput.* **32**, 363 (1978).
2. A. HARTEN AND S. OSHER, *SIAM J. Numer. Anal.* **24**, 279 (1987).
3. A. HARTEN, S. OSHER, B. ENGQUIST, AND S. CHAKRAVARTHY, *J. Appl. Numer. Math.* **2**, 347 (1986).
4. A. HARTEN, B. ENGQUIST, S. OSHER, AND S. CHAKRAVARTHY, *J. Comput. Phys.* **71**, 231 (1987).
5. S. OSHER AND P. K. SWEBY, "Recent developments in the numerical solution of non-linear conservation laws," in *The State of the Art in Numerical Analysis*, edited by A. Iserles, and M. Powell (Clarendon Press, Oxford, 1987), p. 681.
6. C.-W. SHU AND S. OSHER, ICASE Report No. 87-33, 1987; *J. Comput. Phys.* **83**, 32 (1989).
7. C.-W. SHU AND S. OSHER, *J. Comput. Phys.* **83**, 32 (1989).
8. E. KATZER AND S. OSHER, UCLA CAM Report No. 88-14, 1988 (unpublished).
9. A. HARTEN, ICASE Report 87-56 UCLA, August 1987 (unpublished).
10. A. HARTEN, "Preliminary Results on the Extension of the ENO Schemes to Two Dimensional Problems," *Proceedings, international conference on hyperboloc problems, Saint-Etienne, January 1986.*
11. D. K. MAO, "A Treatment of Discontinuities in Shock Capturing Finite Difference Methods I. Single Conservation Law," preprint. 1988 (unpublished).
12. J. F. MCKENZIE AND K. O. WESTPHAL, *Phys. Fluids* **11**, 2350 (1968).
13. P. D. LAX AND B. WENDROFF, *Commun. Pure Appl. Math.* **13**, 217 (1960).
14. P. WOODWARD AND P. COLELLA, *J. Comput. Phys.* **54**, 115 (1984).
15. S. ZALESAK, "A preliminary comparison of modern shock-capturing schemes: Linear advection," *Advances in Computer Methods for Partial Differential Equations, VI*, edited by R. Vichnevetsky and R. Stepleman (IMACS, North-Holland, Amsterdam/New York, 1987).
16. H. YANG, Ph. D. thesis, in preparation.